Industrial Crops & Products 205 (2023) 117407

Contents lists available at ScienceDirect

Industrial Crops & Products

journal homepage: www.elsevier.com/locate/indcrop

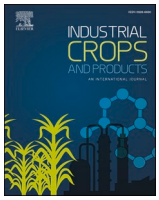

Evaluation of the acid hydrolysis as pre-treatment to enhance the integration and functionality of starch composites filled with rich-in-pectin agri-food waste orange peel

Ana Isabel Quilez-Molina [a,b,*], Leandra Oliveira-Salmazo [a,b], Clara Amezúa-Arranz [a], Alberto López-Gil [a,b], Miguel Ángel Rodríguez-Pérez [a,b,*]

[a] Cellular Materials Laboratory (CellMat), Condensed Matter Physics, Crystallography, and Mineralogy Department, Faculty of Science, University of Valladolid, Spain
[b] BioEcoUVA Research Institute on Bioeconomy, University of Valladolid, Spain

ARTICLE INFO

Keywords:
Starch
Pectin
Orange peel
Biocomposite
Acid hydrolysis

ABSTRACT

The poor management of citrus wastes as a result of their low compostability and value for animal feeding greatly hinders the disposal of this waste. Nowadays, the incorporation of vegetable biomass into a polymer matrix is widely considered as an emerging approach to reduce the environmental problem related to the accumulation and management of food wastes. However, the fibrillar morphology and chemical heterogeneity of biomass usually restrains the compatibility with polymer matrices. Despite that, starch composites containing up to 40 wt % of the neat/hydrolyzed orange peel with excellent mechanical, and moisture resistant features were successfully fabricated in this research. The compatibility between both components was improved by using a simple and scalable process based on the acid hydrolysis of the biomass. Indeed, it was demonstrated that the final properties of these biocomposites were tuned by modifying the acid conditions (type and concentration of acid). For example, composites treated with chlorohydric acid displayed superior Young's modulus values (about 30% more) and slightly greater elongation than the composites composed by 40 wt% of neat orange peel. Moreover, the exposure of vegetable biomass to moderate acid conditions (0.1 and 1 M chlorohydric acid) resulted into the generation of highly-value products, such as organic acids or humic substances, able to form ester bonds with the starch matrix strengthening the water resistance and mechanical features of the composites.

1. Introduction

Starch has been demonstrated to be a great sustainable substitute for polluting petroleum-based polymers with a wide range of application in several fields due to its processability and availability (Fitch-Vargas et al., 2023; Islam and Jiang, 2022; Prachayawarakorn et al., 2011). This biopolymer is mainly found in the stems, roots, and leaves of several vegetables like rice, corn, potato, and wheat, in form of semicrystalline granules (Merino et al., 2022). Chemically, starch granules are based on two polymeric components based on glucose units: linear and long amylose chains, and highly branched amylopectin (Prachayawarakorn et al., 2011). The strong inner structure results into the lack of solubility in cold water and common solvents, which restrains its processability and industrial application (Tian et al., 2022). The gelatinization process implies the disruption of the intermolecular bonds of starch under the application of heat and water that allows fabrication of starch films by casting (Chakraborty et al., 2022; Tian et al., 2022). However, these films are characterized by presenting low water resistance, and poor thermal and mechanical properties (Prachayawarakorn et al., 2011; Toro-Márquez et al., 2018; Zuo et al., 2014). The inherent drawbacks of starch films have prompted the employment of different methods to enhance starch properties. Most of them are based either on the incorporation of fillers as reinforcements or on chemical modifications.

These fillers may come from natural resources such as agri food wastes. The current environmental concern linked to their accumulation and lack of proper end of life management, has prompted new research lines focused on the revalorization of agri-food discards towards the production of more sustainable processes and products (Islam and Jiang, 2022; Merino et al., 2018). In most of cases, vegetables undergo several extractive processes to obtain a product that will be used as an additive

* Corresponding authors at: Cellular Materials Laboratory (CellMat), Condensed Matter Physics, Crystallography, and Mineralogy Department, Faculty of Science, University of Valladolid, Spain.
E-mail addresses: anaisabel.quilez@uva.es (A.I. Quilez-Molina), marrod@uva.es (M.Á. Rodríguez-Pérez).

https://doi.org/10.1016/j.indcrop.2023.117407
Received 3 July 2023; Received in revised form 22 August 2023; Accepted 29 August 2023
Available online 10 September 2023

or filler, like lignocellulosic fibers (Abe et al., 2021; Müller et al., 2014), pectin (Sani et al., 2021), cellulose (Benito-González et al., 2019; Tian et al., 2022), or antioxidants (e.g., anthocyanins, tannins, and gallic acid) (Collazo-Bigliardi et al., 2019; Reinaldo et al., 2021). Many reports have incorporated these extracts to starch films to improve the properties. For example, natural fibers have been demonstrated to be good reinforcements when incorporated into the starch matrix, increasing the tensile strength and Young's modulus (Li et al., 2018; Prachayawarakorn et al., 2011). Moreover, the functional groups of natural fibers interact with the numerous hydroxyl groups located in the starch chains reducing the interaction with water and enhancing the water resistance properties (Li et al., 2018; Quilez-Molina et al., 2022a).

However, the approach based on using the extracts from vegetables wastes still generates a lot of residues that contributes to the environmental problem related to the accumulation of wastes (Merino et al., 2021). The awareness of the environment and circular economy have resulted in some articles that have added the whole vegetable discard into starch matrices, to improve the properties of the starch composites. Some examples are jabuticaba peel(Ribeiro Sanches et al., 2021) and pomegranate peel (Ali et al., 2019b), which enhanced the mechanical properties of starch in both cases. Among whole vegetable discards, orange peel (OP) is very promising since orange represents the most abundant fruit crop in the world (de la Torre et al., 2019; Espinosa et al., 2022). However, its low content of nitrogen and interaction with soil microbiota limits its compostability, while its low pH and anti-nutritional properties avoid its use for animal feeding (Espinosa et al., 2022). Therefore, it is highly important to find other effective valorization routes for this industrial crop. Its chemical composition, rich in biopolymers and active biomolecules, has been widely used for the development of emerging materials in the field of water treatment (Campagnolo et al., 2019) and food packaging (Quilez-Molina et al., 2022b). Indeed, the high content in pectin of OP, which range 30–45%, provides a great film forming capability, allowing the fabrication of films constituted mainly by this agri-food waste (Merino et al., 2021; Quilez-Molina et al., 2022b). Moreover, pectin has shown to have a positive effect on improving the gelatinization properties of starch and hence, its processability (Sani et al., 2021; Y. Zhang et al., 2021). The great compatibility between starch and pectin has allowed the fabrication of active composites by the addition of substances of different nature (e.g., metallic nanoparticles (Sani et al., 2021), plant extracts (Homthawornchoo et al., 2022)). Similarly, the high content of pectin in orange peel has been crucial to allow the fabrication of starch composites containing up to 50 wt% of untreated orange peel with good properties (Chhatariya et al., 2022). However, the mechanical and water sensitivity characteristics of the OP-starch composites reported in Chhatariya et al. (2022) were still far from the conventional materials found in the market, which prompted the research of new strategies for developing sustainable composites with competitive properties.

A preliminary chemical or physical pre-treatment of the whole vegetables wastes has been proven to improve the cohesivity with the starch matrix and enhance the composite properties (Merino et al., 2022). The acid hydrolysis is for instance a good approach which has been previously used to pre-treat the biomass and obtain starch composites with competitive properties (Quilez-Molina et al., 2022a). The acid treatment in vegetable biomass usually entails the disruption of the lignocellulose framework and the generation of low-weight and high value-added chemicals (e.g. sugars, furfurals, and organic acids), very important for the industry (Świątek et al., 2020). Moreover, the hydrolysis of vegetable waste has been widely employed to obtain crystalline cellulose with excellent features to be used as reinforcement of the mechanical and barrier properties of several matrices (Bruni et al., 2020; Chen et al., 2009; Collazo-Bigliardi et al., 2018; Kumar et al., 2020; Trache et al., 2017). Several previous research works have processed vegetable wastes in very different manners, from strong and concentrated inorganic acids like HCl (Gallo et al., 2022; Perotto et al., 2018), to weak organic acids like citric acid (Quilez-Molina et al., 2022b), showing in both cases good film forming capability. Although stronger inorganic acids claim to have a higher hydrolysis effect, the actual tendency is the use of weak organic acids because they are less toxic, more eco-friendly and safety (Gallo et al., 2022). Nevertheless, as far as we know, the influence of the hydrolysis method employed on vegetable discards, as well as its effect on the final properties of the composites obtained have not been deeply analyzed up to date. Therefore, a detailed analysis of the hydrolysis effect on the agri-food discard opens the opportunity to improve the physical properties of starch films by incorporating large quantities of whole agri-food residues.

This work focused on the assessing of the acid hydrolysis as a pretreatment method to obtain novel sustainable corn starch films filled with rich-in-pectin agro-food discards, as it is the whole orange peel, with improved physical properties. For this aim, orange peel was preprocessed using two different types of acids: strong inorganic hydrochloric acid (HCl), and weak and organic acetic acid (Ac) in two different concentrations (0.1 M, and 1 M). Then, the properties of the corn starch films filled with the maximum concentration of biomass analysed in this work (40 wt% of OP with respect to starch) will be evaluated in terms of physicochemical, water resistance, thermal, and mechanical properties. Despite the.

2. Materials and Methods

2.1. Materials

A native corn starch (S) provided by Quimidroga presented 21.0% amylose, 78.94% amylopectin, 0.5% proteins, 0.15% lipids, and 9.30% moisture. This starch was a white powder; a pH in suspension a 20ºC was 4.5–6.0; an apparent density 450–550 g/L, and a Babender viscosity (10 min at 95ºC) was 700 UB. Native corn starch was selected because is cheaper than modified starches (i.e., waxy or high-amylose content), in addition to constituting the major starch source, around the 80–85% of the starch produced worldwide, enabling a future implementation for industrial applications (Palanisamy et al., 2020; R. Zhang et al., 2021). Glycerol provided by Quimidroga and deionized water obtained from a RiOs-DI® 3 Water Purification device were used as plasticizers. Hydrochloric acid, min. 35% extra pure Ph Eur. from Scharlab and Ac solution 50% v/v extra pure from Scharlab were used to chemically treat the orange peel. The orange peel powder was obtained from the oranges discarded after juicing by a local canteen in Valladolid (Spain). According to reported in bibliography (Bizzani et al., 2017; Boukroufa et al., 2015; Merino et al., 2021), the chemical composition neat orange peel powder is rich in polysaccharides such as cellulose (20–40%), hemicellulose (15–25%) and pectin (30–45%). The fruit discard was cut and placed to dry in the oven at 50 °C for 4 days. Then, the fruit peel was grounded to fine powder by a ball mill machine (Ball Mill, Orto Alresa) under room temperature and in presence of two small stainless-steel balls for one minute and 29 Hz. The analysis of the SEM of the OP powder determined a particle size distribution ranging from 10 μm to 170 μm (average size: 65.1 $\pm$ 34.4 μm). The SEM micrographs at different scales and distribution size histograms are reported in **Fig.S1.**

2.2. Preparation of corn starch composites

The fabrication scheme of the starch and starch-OP composites using the solvent casting method is displayed in Fig. 1. This scheme shows that the gelatinization of corn starch was performed in presence of glycerol and different concentrations of OP (0, 10, 20, and 40 wt%, with respect to starch) in two different reaction media: **(a)** with water, **(b)** with HCl or Ac acid in 1 M or 0.1 M. For the route **(a)**, starch (6 wt%), glycerol (3 wt%), and the additive OP were poured into 100 mL of water. After adding all reagents, the solution was stirred at 300 rpm on a hot plate for 25 min under temperature control to induce the starch gelatinization and to ensure the proper mixing of the components. Under these processing conditions, the solution temperature increased from room

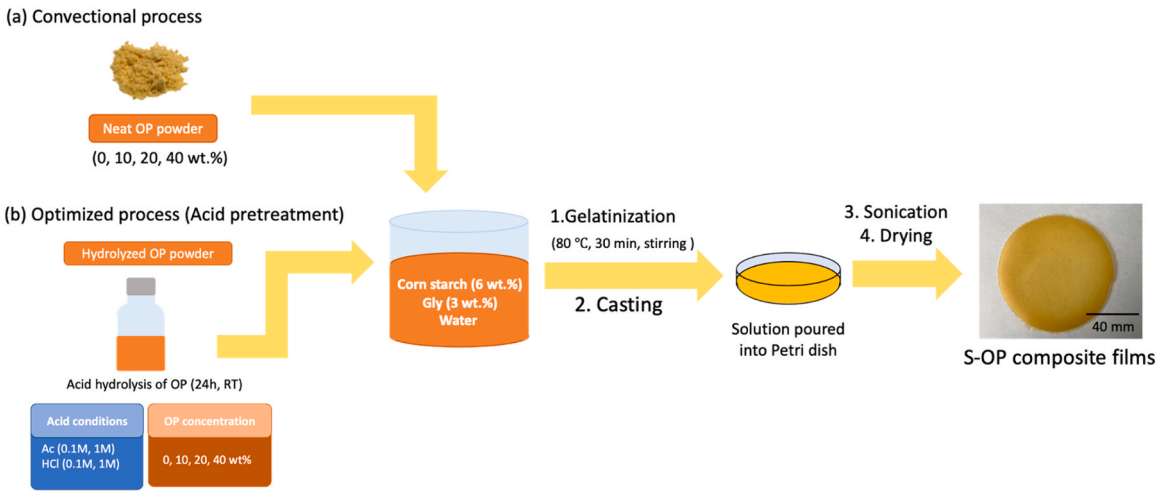

Fig. 1. The scheme of the fabrication process of S and S-OP composites films using **(a)** convectional method, and **(b)** proposed method (with the acid pretreatment).

temperature (~25ºC) to a maximum of 90 ºC. Herein, the opaque solution became clear and viscous indicating that the gelatinization process occurred (T_{onset} ~80 ºC). The gel was cast onto a standard 90 × 14 mm plastic Petri dish. After that, the petri dishes containing the casted composites were carefully placed on a stainless tray in a sonication bath for 15 min at 50 kV to eliminate the remaining bubbles formed during the gelatinization process. For this step, the bathwater level was decreased to avoid that the bathwater enters in contact with the sample. Ultimately, samples were left to dry (25ºC, 40% relative humidity) for 24 h, obtaining films with an average thickness of about 0.35 mm. After drying, films were kept at room conditions (25ºC, 40% relative humidity) until their analysis for a maximum 3 months.

For the preparation of S-OP composites, the route **(b)** includes a new pre-treatment step that consists of the hydrolysis of the OP powder. Herein, the desired concentration of OP (10 wt%, 20 wt%, and 40 wt%, with respect to the starch) was put to stir with 20 mL of acid (0.1 M, 1 M of HCl or Ac) for 24 h at room temperature. Then, the acid solution containing the hydrolyzed powder was poured into the aqueous solution of 6 wt% starch and 3 wt% glycerol. This resulted into a final solution with an acid concentration of 0.1 M and 0.01 M, for the poured solution of 1 M and 0.1 M, respectively. It's worth mentioning that the antiseptic properties of acids will aid to avoid the growth of microorganism or moulds in the films during the drying process, as proven elsewhere (Ma et al., 2022). These acids were selected as representative examples of strong inorganic acids (i.e., HCl) and weaker but greener and safer organic acids (i.e., Ac) because they do not trigger additional chemical modifications to the starch and lignocellulose components. For example, the treatment of native starch with citric acid or oxalic acid commonly results into cross-linking or esterification reactions, modifying the material functionality and hindering the study of the effect of the acid hydrolysis on the final properties of the composites (Gebresas et al., 2023; Karma et al., 2022; Menzel et al., 2013). Moreover, Ac is volatile, which ensure the complete elimination of any residual trace in the matrix (Quilez-Molina et al., 2022a). HCl exhibits stronger hydrolytic capability with respect to other inorganic acids, such as dibasic or tribasic acids (e.g., H_2SO_4 or H_3PO_4) (Singh and Ali, 2008). With the aim of understanding the effect of the acid (diluted) on the starch gelatinization and film properties, another batch of samples without orange peel were fabricated adding 20 mL of acid solutions of 0.1 M, 1 M of HCl or Ac. This corresponded with a reaction solution with a final acid concentration of about 0.01 M and 0.1 M, respectively. Films were fabricated following all the steps explained above.

Table 1 displays the labelling and chemical composition of some representative samples. As observed, the content used of starch, glycerol and water were the same for all films: starch (6 wt%), glycerol (3 wt%), and 100 mL of water. The process proposed in this manuscript entailed the addition of 20 mL of acid (Ac or HCl) in different concentrations to promote the hydrolysis of the biomolecules present in the starch or orange peel. The Table S1 of Supporting information collects the information of all the samples fabricated in this work.

2.3. DSC of the heat-moisture process

The thermal properties were characterized by differential scanning calorimetry (DSC) using a Mettler DSC30 differential-scanning calorimeter (Mettler-Toledo, Columbus, OH, USA). The specimens were

Table 1
Labelling and composition of some representative samples.

Labelling	Reagents	Reaction medium			Orange peel	
	S (6 wt%) Gly (3 wt%)	**Only water (100 mL)**	**Water (100 mL) + Acid solution**	**Additive concentration (wt %)**	**Neat**	**Pre-treated**
S	Yes	Yes	No	No	No	No
S_10OP	Yes	Yes	No	10	Yes	No
S_40OP	Yes	Yes	No	40	Yes	No
S_0.1Ac	Yes	No	20 mL of 0.1 M Ac	No	No	No
S_0.1Ac_40OP	Yes	No	No	40	No	20 mL of 0.1 M acetic acid
S_1Ac	Yes	No	20 mL of 1 M Ac	No	No	No
S_1Ac_20OP	Yes	No	No	20	No	20 mL 1 M Ac
S_1Ac_40OP	Yes	No	No	40	No	20 mL 1 M Ac
S_0.1HCl	Yes	No	20 mL of 0.1 M HCl	No	No	No
S_0.1HCl_40OP	Yes	No	No	40	No	20 mL 0.1 M HCl
S_1HCl	Yes	No	20 mL of 1 M HCl	No	No	No
S_1HCl_40OP	Yes	No	No	40	No	20 mL 1 M HCl

heated from 0ºC to 105ºC at a heating rate of 5ºC/min in nitrogen atmosphere. The raw mixtures containing starch powder, orange peel (neat or hydrolyzed), water and glycerol, were measured in triplicate, and the gelatinization temperature (Tgel) obtained for each sample was represented in terms of average ± standard deviation (SD).

2.4. Morphology study: Scanning electron microscopy (SEM)

The morphology study of the starch films was performed by SEM microscopy using a FEI ESEM Quanta 200 Felmi-ZFE (Steyrergasse, Austria) equipped with EDX EDAX Genesis AMETEK inc (Whitsett, EE. UU). The morphology of the starch-orange peel films was analyzed both on the films surface and on the cross-section. For the cross-section analysis the samples were previously cooled down under liquid nitrogen and fractured. All samples were coated with gold (10 nm thickness layer) and the measurement was performed using an accelerating voltage of 10 kV and a secondary electron detector (SED).

2.5. Chemical study: Fourier transform infrared (FTIR)

The infrared spectra of the starch-orange peel films was collected using Bruker Tensor 27 Spectrometer working in the Attenuated Total Reflectance (ATR) method with an MKII Golden-Gate accessory. Each FTIR spectrum was obtained at room temperature after 64 scans, with a resolution of 4 cm^{-1} in the range 4.000–600 cm^{-1}. The infrared peaks of the samples were normalized using the peak that corresponded to the stretching vibration of the glycosidic group, υ(C-OH), at 1010 cm^{-1} (Terzioğlu et al., 2021).

2.6. Crystallinity study

The X-ray patterns of S films and S-OP composites were acquired using a Bruker Discover A25 diffractometer equipped with a 2.2 kW Cu Kα ceramic X-ray tube and a LynxEye detector operating at 40 kV and 30 mA. The diffraction patterns were collected in parallel beam geometry and symmetric reflection mode using a zero-diffraction silicon substrate over an angular range of 2θ = 5–80º and a step size of 0.02 º. The crystallinity index (IC) was calculated using the method and Eq. 1 reported by (Quilez-Molina et al., 2022a):

$$CI = \frac{A_c}{A_{total}} \quad x100 \tag{1}$$

Where A_c is the area of the crystalline phase, and A_{total} is the overall area.

2.7. Thermogravimetric analysis

Thermal gravimetric analysis (TGA) was performed using a SDTA851, Metter Toledo (Barcelona, Spain) instrument. The temperature program was set in a range from 50 ºC to 850 ºC under N_2 (60 mL/min) and a ramp temperature of 20ºC/min.

2.8. Moisture content

The moisture content was measured by introducing the samples (~2 cm^2) with a weight (W_1) in a vacuum oven at 40 ℃ until reaching constant weight (W_2). The moisture content was calculated following the Eq. 2 below (Quilez-Molina et al., 2022b):

$$Moisture \quad (\%) = \frac{W_1 - W_2}{W_1} \quad x100 \tag{2}$$

All samples were measured in triplicate, and results were represented in terms of average ± standard deviation (SD).

2.9. Solubility

The solubility was calculated by introducing film pieces (~2 cm^2) and with a weight (W_1) in 15 mL of distilled water for 24 h at room temperature (20 ± 5 ℃). The residual films were separated using tweezers and dried in a vacuum oven at 40 ℃ for 24 h until constant weight (W_2). The solubility was calculated according to the following Eq. 3:

$$Solubility \quad (\%) = \frac{W_1 - W_2}{W_1} \quad x100 \tag{3}$$

All samples were measured in triplicate, and results were represented in terms of average ± SD.

2.10. Moisture adsorption

The moisture adsorption measurements were carried out under 75% RH (relative humidity) at 25 ℃. Prior to the experiment, all samples (~2 cm^2) were dried under vacuum oven at 40 ℃ until achieving a constant weight (W_0). Then, the samples were placed into a sealed chamber with the desired humidity conditions (75%) using supersaturated salts according to ASTM E 104–2 and weighted at different time intervals (W_t) until a constant weight was attained. The moisture adsorption was calculated using the following formula (Eq. 4) according to the article reported by Wan Y.Z. et al., (Wan et al., 2009).

$$\text{Moisture uptake}(\%) = \frac{W_t - W_0}{W_0} x100 \tag{4}$$

All samples were measured in triplicate, and results were represented in terms of average ± SD.

2.11. Mechanical properties

The tensile tests were performed using a Universal testing machine model 5.500R6025 Instron. For these tests, Dog-bone-shaped samples were cut from the films and air-conditioned at the same room conditions (50% of relative humidity) at temperature of 23 ± 2 ºC and RH of 50 ± 10% during 24 h prior to the measurement. The samples were stretched under a strain rate of 10 mm/min. The study of the tensile-strain curves provided the values of Young's modulus (YM), tensile strength (TS), and elongation at break (E) using the built-in software of the tensile tester. At least three measurements were taken for each sample, and the results were expressed as average ± SD.

3. Results and discussion

3.1. Chemical study of the orange peel powder hydrolysis

The chemical changes undergone in the orange peel during the hydrolysis pre-treatment was evaluated through infrared spectroscopy. The infrared spectra with the band assignments are reported in Fig. 2**(a)**. All OP powdered samples exhibited the characteristic infrared peaks attributed to holocellulose and pectin, like other citrus biomass reported in bibliography (Chhatariya et al., 2022; Quilez-Molina et al., 2022b; Terzioğlu et al., 2021). The strong band placed at 3300 cm^{-1} was assigned to the stretching vibration of the hydroxyl groups present in carbohydrate fraction, while the asymmetric and symmetric stretching vibration bands of C-H of the aliphatic groups were located at 2975 cm^{-1} and 2950 cm^{-1} (Quilez-Molina et al., 2022b; Terzioğlu et al., 2021). The vibration peaks of the carbonyl (C═O) was at 1735 cm^{-1}, while the peaks located at 1610 cm^{-1} and 1410 belonged to the asymmetric and symmetric vibration of the carboxylate group (COO^-), respectively (Merino et al., 2021; Quilez-Molina et al., 2022b). The vibration peaks ranged from 1300 cm^{-1} to 1000 cm^{-1} corresponded to the stretching vibrations (C-C, C-O, C-OH) associated with the glycosidic linkages (Szymanska-Chargot and Zdunek, 2013; Terzioğlu et al., 2021).

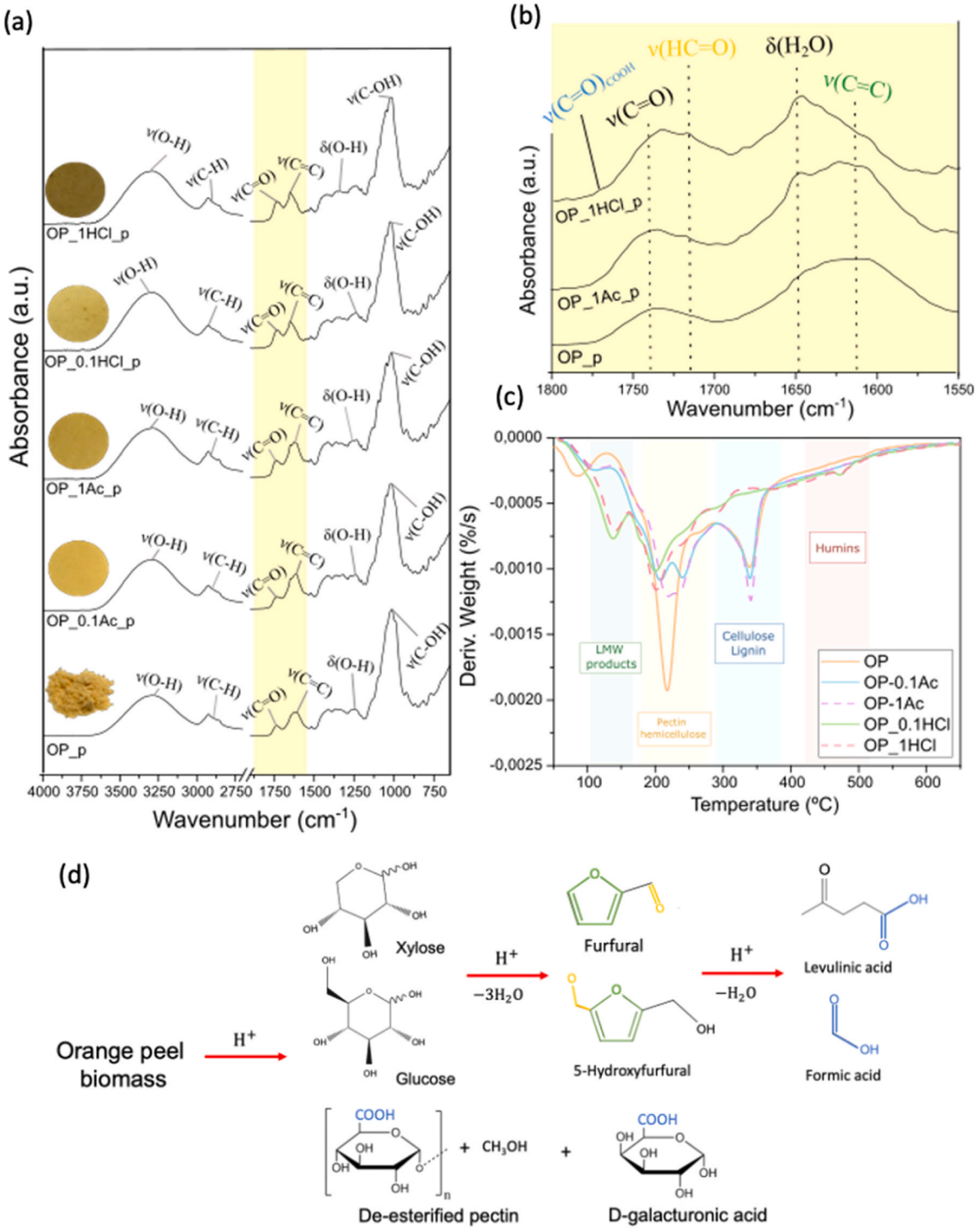

Fig. 2. **(a)** Infrared spectra of the orange peel powder treated at different acid conditions. **(b)** The infrared spectra of neat OP powder, and OP powder treated with acetic and chlorohydric acid at 1 M maximized in the range 1800–1550 cm^{-1}. Photographs of OP powder casted after the treatment with 20 mL of 0.1 M Ac, 1 M Ac, 0.1 M HCl, 1 M HCl in the inset. **(c)** Derivative curves of the thermal degradation of hydrolyzed orange peel. **(d)** Scheme of the chemical reactions occurred in the biomass.

The inspection of the infrared spectra of the orange peel powders processed at different conditions revealed significant differences associated to the acid hydrolysis. In general, the band related to the hydroxyl group increased in all hydrolyzed samples, as a result of the cleavage of the hydrocarbon chains (pectin and hemicellulose, but also cellulose to the least extent) to form saccharides with lower molecular weight (Mohamad et al., 2020; Quilez-Molina et al., 2022b; Sila et al., 2009). Only samples treated with acids, both Ac and HCl, at 1 M concentration exhibited relevant chemical changes in other ranges of the infrared spectra. At these conditions, the de-esterification and subsequent hydrolysis of the pectin fraction of the orange peel occurs, resulting into chains of lower-molecular-weight de-esterified pectin and D-galacturonic acid (Kurita et al., 2008). Moreover, the exposure of vegetable biomass to moderate acid conditions can led to the oxidation and condensation of the organic matter towards the formation of humic substances (Mohamad et al., 2020; Valdivieso Ramirez et al., 2021; Yu

et al., 2021). The presence of the latter can be determined by assessing the vibration bands located in the region 1800–1550 cm^{-1}, maximized for neat OP, OP_1Ac_p and OP_1HCl_p in Fig. 2**(b)**. In this section of the spectra is observed an increment of the band at 1735 cm^{-1}, related to the carbonyl groups, which confirmed the transformation of polysaccharides into more oxidized species (Yu et al., 2021). A new peak appeared at 1715 cm^{-1} corresponding to the stretching vibration of the aldehyde group (HC═O) presents in humic substances like furfural or hydroxymethylfurfural (Mohamad et al., 2020; Pin et al., 2014; Valdivieso Ramirez et al., 2021; Yu et al., 2021). The formation of these dark brown coloured organic products was also supported by the visible color change of the sample (Dwyer et al., 2008; Merino et al., 2021), as easily observed in the photographs in Fig. 2**(a)**. The peak at 1650 cm^{-1} corresponded to the bending vibration of water absorbed after the acid treatments (Szymanska-Chargot and Zdunek, 2013), while the new bands placed in the range from 1550 to 1500 cm^{-1} belonged to the formation of the aromatic furan ring of the furfural and hydroxymethylfurfural (Pin et al., 2014; Yu et al., 2021). Finally, the infrared spectra of samples hydrolyzed with HCl exhibited a small new band at 1760 cm^{-1}. This band corresponded to formation of organic acids, indicating that these moderate conditions led to the last step of the biomass degradation (Mohamad et al., 2020; Valdivieso Ramirez et al., 2021; Yu et al., 2021). Moreover, this band corresponded also with the hydrolysis and de-esterification of pectin, which results into the formation of new carboxylic acid groups (Kurita et al., 2008).

The DTG of OP and OP hydrolyzed are reported in Fig. 2**(c)**. The TG curves and the residual weight are reported in Fig. S2, in Supporting information. The thermograms of OP powder indicated that the degradation occurred in four stages, like reported in the literature (Açıkalın, n.d.; Merino et al., 2021). From ambient temperature to below 100 ℃, the ~5% of mass was lost due to dehydration of the biomass (Salasinska et al., 2018). The second degradation step occurred in the range of 128–288 ℃, while the third degradation step took place from 288 ℃ to 338 ℃, with a mass loss of ~37% and ~31%, respectively. The two last degradation stages were attributed to the decomposition of the main structural polymeric components of the OP. In particular, hemicellulose and pectin degraded at first, followed by the cellulose and lignin, which degraded at the end of the thermal treatment (Açıkalın, n.d.; Merino et al., 2021). The final residue was 28%, in agreement with what was reported in other articles (Açıkalın, n.d.). The maximum-mass loss rates were measured at 280℃ and 340℃, in the second and third degradation state. In the same graph, the thermograms of hydrolyzed OP indicated that the thermal degradation greatly varied with the type of acid. The thermal degradation profiles of Ac-hydrolyzed samples were very similar to neat OP, with only visible changes in the second degradation peak (~220℃), related to the degradation of pectin and hemicellulose. The peak shifting towards higher temperatures suggested the formation products with a higher thermal stability as a result of the chemical reaction between the Ac and these biopolymers (Boluda-Aguilar and López-Gómez, 2013). The thermal degradation peak related to the cellulose and lignin was kept similar indicating that Ac barely altered these two last components. The thermograms of HCl-hydrolyzed OP displayed a new first degradation stage at lower temperatures (95–160 ℃) with a mass loss of 10%. This step could be related to the formation of low-molecular weight (LMW) products as a result of the hydrolysis of the biopolymers chains (Merino et al., 2021). Indeed, the low weight loss observed in the thermal decomposition of the different biopolymers indicated the cleavage of the biopolymer chains during the acid treatment. Interestingly, a small peak at 420℃ in these samples confirmed the presence of high-thermal resistant humins as a result of the acid hydrolysis reactions represented in Fig. 2**(c)** (Liu et al., 2018). The weight of the residue increased with the strength of the acid hydrolysis, from 28% in neat OP to 34% in OP_1HCl, indicating that the reaction with acids generated more thermal resistant products, see Fig. S2 in Supporting information.

All the reaction schemes of the chemical processes abovementioned are displayed in Fig. 2**(d)**. In the humic substances, the aldehyde and furfural groups are highlighted in yellow and green, respectively. The carboxylic acid group belonged to the final organic acids, de-esterified pectin and D-galacturonic acid is colored in blue.

3.2. Analysis of the heat-moisture process through DSC

The effect of orange peel (neat and hydrolyzed) on the starch gelatinization was determined by comparing the DSC thermograms of the raw-mixtures (starch powder, neat or hydrolyzed orange peel powder, glycerol and water) reported in Fig. 3, starch with 40 wt% of OP and starch with 40 wt% of OP hydrolyzed with 1 M HCl. The starch thermogram presents an only peak around 60–80 ℃ attributed to the gelatinization process (Y. Zhang et al., 2021). The addition of orange peel (present in neat and hydrolyzed form) induced an increment of the gelatinization temperature (Tgel) from 70.03 ± 0.01 ℃, observed in starch only, to a maximum of 71.89 ± 0.18 for S_1HCl_40OP ℃. This phenomenon was attributed to the high content in pectin of the orange peel. It is well known that pectin biopolymer penetrates starch granules, interacting through hydrogen bonding with starch chains and promoting structural changes of the starch granules (Y. Zhang et al., 2021). The further increment of the gelatinization temperature with the hydrolyzed additive could be a consequence of the formation of smaller molecules that can penetrate easier into the swelled granule and interact with starch chains (Y. Zhang et al., 2021). Therefore, this result highlighted the good compatibility between both components. The stronger hydrolytic capability of HCl against Ac could explain the higher gelatinization temperature.

3.3. Film-forming capability of samples

The good properties of corn starch to form films using water as solvent for the dilution and gelatinization has been well documented (Ali et al., 2019b, 2019a; Bodirlau et al., 2013; Chakraborty et al., 2022; Zhang et al., 2011). The photographs of S films and corn S-OP composites (OP present in 10, 20, and 40 wt% with respect to the starch) treated under different acidic conditions are reported in Fig. 4**(a-d)**. It is worthy notice that the addition of higher contents of OP might result into films with physicochemical characteristics more similar to agri-food discard than starch, and they will be no longer starch-based composites. However, the properties obtained in films containing 40 wt% of OP will be compared with films 100% based of acid hydrolyzed orange peel reported in a previous work (Quilez-Molina et al., 2022b), in the following sections. The film thickness is reported in the down right side of the picture. All films reported in Fig. 4 exhibited a good appearance, with no fractures or grooves, confirming the suitability of the fabrication

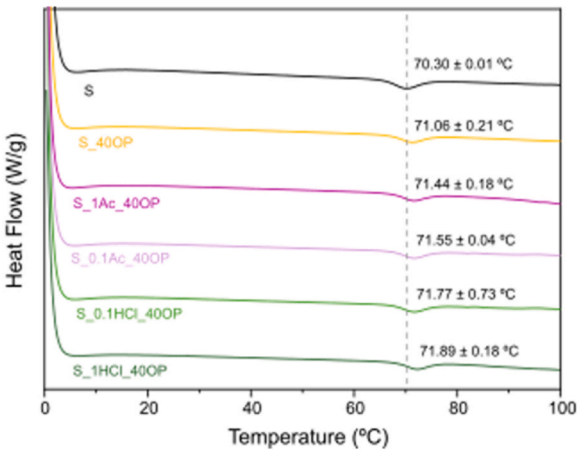

Fig. 3. Differential scanning calorimetry thermograms of the starch, and starch composites loaded with 40 wt% of OP.

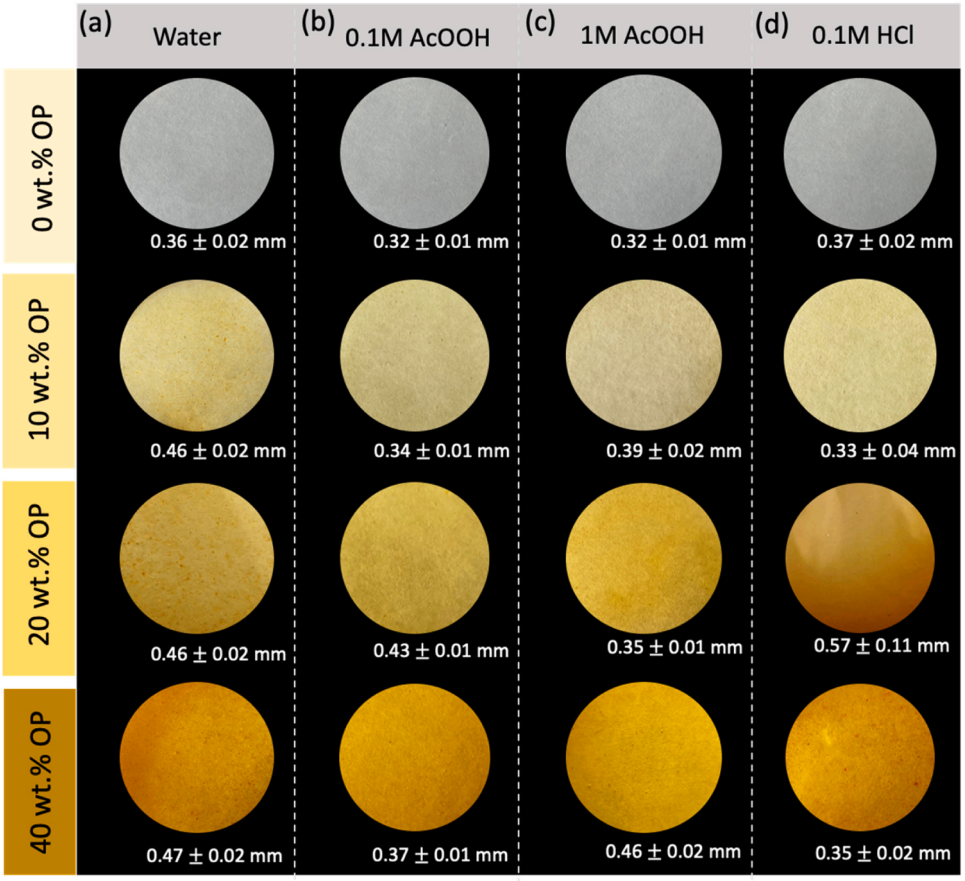

Fig. 4. Photographs and thickness of samples with film forming properties and containing **(a)** orange peel and orange peel treated with **(b)** 0.1 M Ac, **(c)** 1 M Ac, and **(d)** 0.1 M HCl.

conditions employed. The photographs revealed that neat samples (without filler) were uncolor, while the addition of OP provided a strong orange coloration that gradually increased with the filler content. This effect was because OP is rich in natural colorants, like quercetin and rutin, with powerful antioxidant and antimicrobial properties (Chhatariya et al., 2022; Ivanovska et al., 2022). Interestingly, in films processed with water, OP particles and agglomerates were easily differentiated with the naked eye. However, these visual defects were barely visible in films containing hydrolyzed OP (processed with acids). This may evidence that the acid hydrolysis favours the filler integration and cohesiveness with the matrix. Moreover, the films treated with 0.1 M HCl acquired a brownish coloration, which increased in samples treated with stronger acid conditions (i.e.,1 M HCl), see Fig. S3 of Supporting information. This color change was related with the hydrolysis of sugars, which dark reaction products (e.g., humic substances) provide a browning coloration to the sample (Dwyer et al., 2008; Merino et al., 2021).

The positive effect of using acids on improving the processability of starch has been documented before in many articles (Chang et al., 2006; Chung and Lai, 2007; Zhang et al., 2011). The acid hydrolysis preferentially occurs in the amorphous regions of the starch; however, acids are also capable to disrupt the α-(1→6) bonds of the amylopectin (Martins and Martins, 2021; Singh and Ali, 2008). As a result of the latter, amylose leaks from the amorphous region of the biopolymer to the aqueous phase (Utrilla-Coello et al., 2014; Y. Zhang et al., 2021). Indeed, Fig. S3 showed that samples treated with 1 M of HCl, which did not form films but gel-like mass, which presented some white precipitates of amylose distributed throughout the surface as a result of the strong hydrolysis reaction. Interestingly, the white amylose precipitates on the surfaces decreased with the OP content. This effect was associated to the high content in pectin of OP, which has been demonstrated that interacts with amylose and amylopectin chains, retarding the leaching (Y. Zhang et al., 2021). In addition, the exposure of new functional groups resulting from the acid hydrolysis of the biomass (Fig. 2**(d)**), which are available to interact with starch biopolymers, likely also contribute to the starch cohesion. These results were in concordance with DSC analysis abovementioned (Fig. 3). According to the fabrication method described in the 2.2 section, the acid concentration of the gelation medium (20 mL 1 M HCl + 100 mL of water) is equivalent to 0.16 M HCl. This result evidenced the high sensitivity of starch to acids, acting as a limiting agent in this processing strategy. Under this basis, the employment of highly hydrolyzed vegetables with acids for the fabrication of starch composites must include an intermediate step of acid neutralization or removal.

3.4. SEM images of films

The surface image of the starch films and orange peel-starch composites are summarized in Fig. 5**.** Neat starch films exhibited a rough surface with some particles which may be broken starch granules, as pointed with red arrows in Fig. 5, indicating a possible incomplete gelatinization (Ma et al., 2009; Otàlora Gonzàlez et al., 2020). These particles disappeared when the starch is formed under acid conditions, demonstrating the acid had a positive effect on the dispersion and homogenization of the matrix, as observed in other works (Martins and Martins, 2021). The noticeable increase in roughness of samples processed with Ac (0.1 and 1 M), against the smooth surface of S_0.1HCl films, was associated to the high evaporation rate/volatility of the organic acid (Strawhecker et al., 2001). As expected, the incorporation of high quantities of OP (40 wt%) involved the increment of roughness

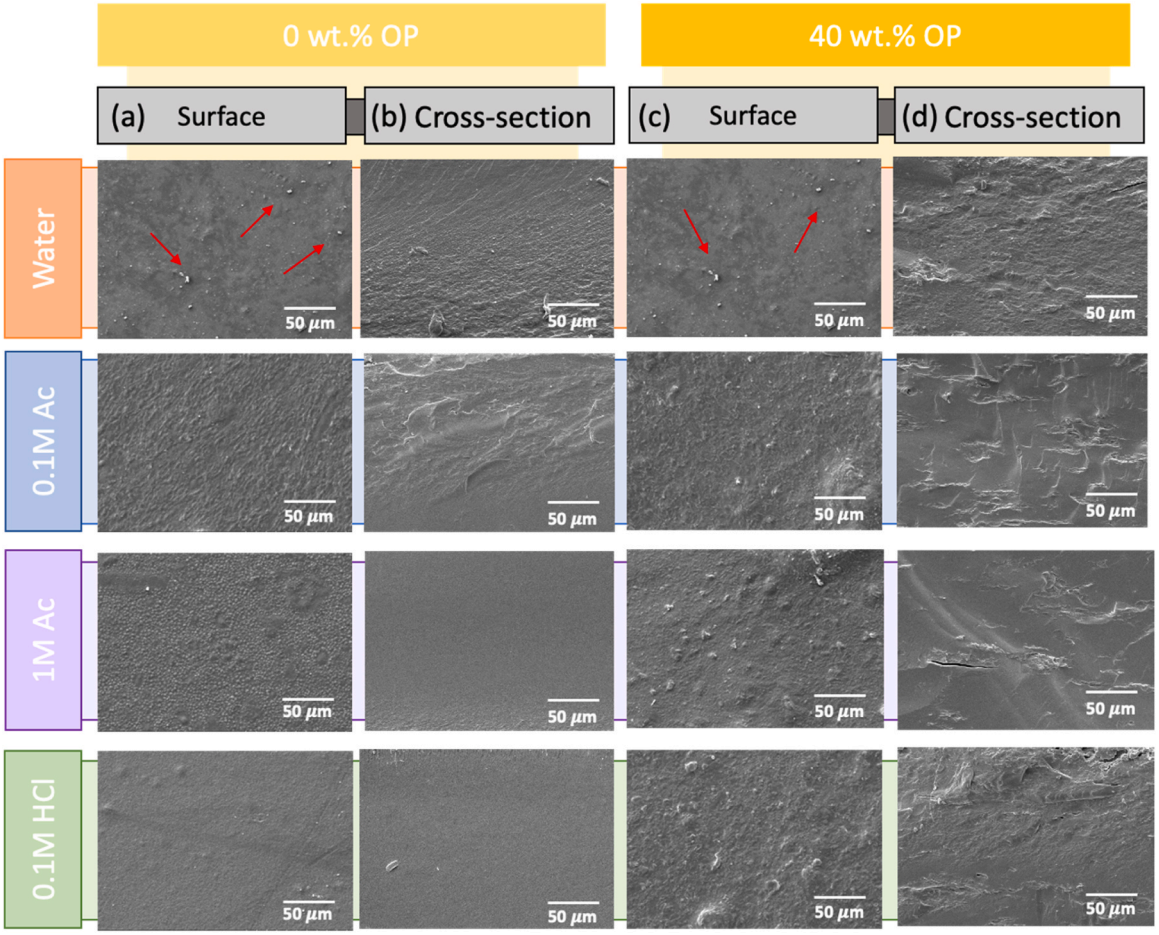

Fig. 5. The SEM images of the **(a)** surface and **(b)** cross-section of S samples treated under diverse acid conditions. The SEM images of the **(c)** surface and **(d)** cross-section of S samples with 40 wt% of OP treated under diverse acid conditions. The grains of broken starch are pointed with red arrows.

in films surfaces. All samples, including films containing 40 wt% of OP, exhibited a compact and rougher cross-section, without important void formation. Generally, the presence of fibers in the vegetable additive restrains the cohesion by the entanglement of the fiber with the matrix (Li et al., 2020). Indeed, in most of the cases found in literature (Lopez-Gil et al., 2014; Otàlora Gonzàlez et al., 2020), starch composites present a poor matrix-fiber interfacial adhesion, even at low contents of natural fibers additives. Despite that, lignocellulose fibers were barely observed within the polymer matrix in the cross-section images of films containing 40 wt% of OP. This indicated that a good dispersion of the additive and compatibility between the two components were successfully achieved, which may be due to the presence of high amounts of pectin in the orange peel. A better view of the good integration of the fibers is provided in the cross-section images acquired at lower scales reported in Fig. S4 of Supporting information.

3.5. Chemical study of S-OP composites

The infrared spectra of S film and S-OP composites with the corresponding peak assignments are displayed in Fig. 6**.** The infrared spectra of neat S films and S films fabricated under different acid conditions displayed in Fig. 6**(a)** exhibited the typical vibration bands of S. The strong vibration band at 3300 cm^{-1} indicated the presence of hydroxyl groups of the polymer chain and plasticizer glycerol. The asymmetric and symmetric stretching vibrations, ν_a(C-H) and ν_s(C-H), of the CH_2 group in the glucose units were located at 2920 cm^{-1} and 2870 cm^{-1}, respectively (Merino et al., 2019; Quilez-Molina et al., 2022a). The peak at 1650 cm^{-1} was assigned to the adsorbed water molecules, while the strong peaks ranging from 1470 cm^{-1} to 1350 cm^{-1} were attributed to the bending vibrations of C-H bonds (Quilez-Molina et al., 2022a; Szymanska-Chargot and Zdunek, 2013). The stretching peaks related to the skeletal glucose, ν(C-O), ν(C-C), and ν(C-O-H), were in the 1100–1150 cm^{-1} range, while the bending peak ν(C-O-H) was at 1100 cm^{-1} (Merino et al., 2019; Warren et al., 2016). The only noticeable difference observed between the hydrolyzed starch films was the emergence of a new weak peak at 1725 cm^{-1} in the infrared spectra of the S_1HCl sample. In literature, this peak has been associated with the carbonyl group of the aldehyde (HC═O) as a result of the oxidation of the starch monomers due to the strong acid conditions (Zuo et al., 2017). This chemical reaction could explain the lack of the film forming capability of the sample, and the formation of low-weight starch precipitates observed in the sample, see Fig. S3 of Supporting information. In Fig. 6**(b)**, the infrared spectra of the S composites loaded with 40 wt% of OP fabricated under diverse conditions were represented. All films displayed the characteristic peaks of the corn S, with slight variations. This result was associated to the high chemical similitudes between both natural components (starch and orange peel biomass), as observed in other starchy composites enriched with plant-based fillers (Quilez-Molina et al., 2022a; Wei et al., 2022). Interestingly, the infrared spectra of S_0.1HCl_40OP and S_1HCl_40OP exhibited a new peak at 1750 cm^{-1}, characteristic to ester group (OC═O), which suggested the esterification of starch chains as a result of the formation of organic acids during the hydrolysis process of the orange peel (see reaction scheme of Fig. 2**(d)**) (Fonseca-Florido et al., 2018; Morán et al., 2013). Moreover, the esterification of starch with OP components could also support the decrease of starchy precipitates in S_1HCl with the orange peel content (See

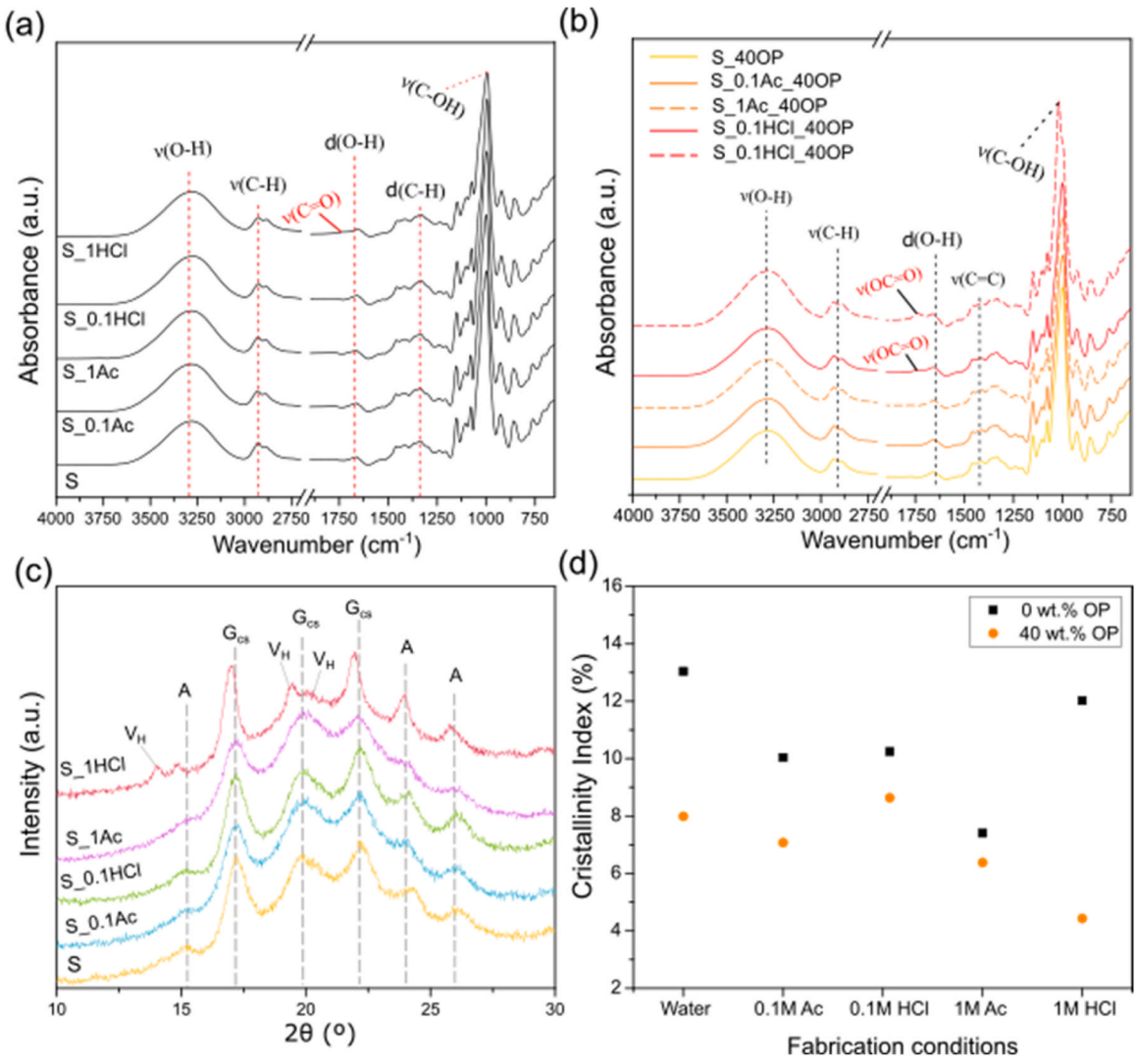

Fig. 6. The infrared spectra and peak assignments of the **(a)** S films and **(b)** S-OP composites treated under different acid conditions. **(c)** XRD patterns of S films and **(d)** Crystallinity index of S (in black) and S-OP composites (in orange) treated under different acid conditions.

Fig. S3 of Supporting information). The lack of noticeable changes in the infrared spectra of the starch composites treated with Ac indicated the lack of relevant chemical changes.

The study of the crystallinity through XRD analysis was performed to provide a more complete information about the inner structure of the plasticized starch. The XRD diffractograms of the diverse plasticized starch obtained without additive are represented in Fig. 6**(c).** The X-ray diffractograms of the plasticized S films displayed a semi-crystalline structure with sharp peaks corresponding to the two main components: amylopectin (crystalline region) and amylose (amorphous region) (Altayan et al., 2017). The main diffraction peaks positioned at 17.2º, 19.9º, and 22.2º coincided with typical X-ray pattern of gelatinized plasticized corn starch (G_{CS}) (Fitch-Vargas et al., 2023; Teacă et al., 2013). However, the presence of characteristic peaks of A-form (15.3º, 24º, 26º), associated with the native corn starch (without plasticization), are also present in the diffractograms (Teacă et al., 2013). This indicated that the plasticization was not complete during the mixing process and reveals that samples preserved the original crystalline structure to a small extent (Ismail et al., 2019; Osman et al., 2020). The small fragments of starch granules observed in the SEM micrographs of neat S films reported in Fig. 5 support this result (Ma et al., 2009). The values of crystallinity (CI) plotted in Fig. 6**(d)** revealed that the weak conditions of acid hydrolysis promoted the loss of crystallinity of the starchy films. This decrement has been reported in other articles and it has been attributed to the disruption of the native A-type structure (Ma et al., 2009; Teacă et al., 2013). On the other hand, when starch was exposed to stronger hydrolysis conditions (1 M HCl), X-ray peaks appeared shaper and more intense, indicating an increment of the crystallinity. This occurred because the inorganic acid disrupted the amorphous region of the starch, breaking several chains and increasing the amount of crystalline regions (Martins and Martins, 2021; Utrilla-Coello et al., 2014). Moreover, the X-ray peaks were shifted, and new peaks related to V_H-type complex (14º, 19.4º, 20.1º) arose, indicating that the concentrated acid had a strong effect on the chain arrangement (Altayan et al., 2017; Osman et al., 2020; Teacă et al., 2013). Literature reports that acid hydrolysis can triggers the polymorphic transition of the XRD patterns that can justify these changes observed in the diffractogram (Wang and Copeland, 2015). As result, this sample exhibited higher crystallinity (~12%) with respect to the other hydrolyzed samples (8–10%), see Fig. 6**(d)**.

The X-ray diffractograms of the samples containing 40 wt% of OP do not exhibit new peaks, see Fig. S5 of Supporting information. However, the crystallinity of samples slightly decreased when orange peel was incorporated, see Fig. 6**(d)**. This could be attributed to the high content in amorphous pectin of the additive (Khorasani and Shojaosadati, 2017). The decay of crystallinity was greater in the sample treated with 1 M

HCl, from 12% (without additive) to 4% (with 40 wt% of OP), as result of the esterification reaction between the starch and carboxylic acids obtained from the biomass hydrolysis (Zuo et al., 2013). The CI obtained was similar to other starch-based composites enriched with natural compounds, such as iota-carrageenan (CI=12–5.8%) (Abdillah and Charles, 2021), and microcrystalline cellulose (CI=7–9.2%) (Area et al., 2019).

3.6. Mechanical properties

The tensile stress-strain curves of each sample are represented in Fig. 7, while the values of tensile strength (TS), elongation or strain to break (ε_R) and Young's Modulus (E) are represented in Table 2. From a first sight, the acid treatment showed to be very important to define the final properties of the S films. In Fig. 7**(a)**, the strength and E of the S films increased with the content of the OP, while the elongation decreased. In Fig. 7**(a)**, the strength and E of the S films increased with the content of the OP, while the elongation decreased. This trend is commonly observed in composites enriched with vegetable-based fillers due to its high content of rigid molecules (such as cellulose and lignin), which can restrict physically the mobility of the polymer chains during the stretching (Chhatariya et al., 2022; Otàlora Gonzàlez et al., 2020). For example, tea waste extract, rich in cellulose and polyphenols, reduced the elongation at break of PVA from ~140% to below 10% (Quilez-Molina et al., 2020). The chemical composition of orange peel, rich in pectin and low in rigid lignin, strongly contributed to significantly preserve the elasticity of the samples even at high concentrations (40 wt%) (Merino et al., 2021; Perotto et al., 2018). Furthermore, the high concentration of filler can be reached due to the great chemical similarities between starch and orange peel, which favorize the proper dispersion of the filler within the matrix, reducing the formation of filler aggregates that act as breaking point (Li et al., 2018; Müller et al., 2014). Interestingly, in comparison, the films composed by 100% orange peel were slightly stiffer, displaying a maximum elongation of 35% and tensile strength (TS) of 7–10 MPa, while the composites reported in this manuscript showed a maximum of 7 MPa (TS) but with an elongation that overcame the 60% in some of the samples (Quilez-Molina et al., 2022b).

The effect of the acid was clearly evidenced in all samples without filler, see black line of Fig. 7**(b,c,d)**). Films fabricated with weaker acid

Table 2
The mechanical parameters TS, ε_R, and E expressed as the mean ± standard deviation of **(a)** S films **(b)** S_0.1Ac, **(c)** S_1Ac, **(d)** S_0.1HCl with different concentration of OP.

Sample	TS (MPa)	ε_R (%)	E (MPa)
S	4.6± 0.1	85.9± 2.5	37.6 ± 2.5
S_10OP	4.5 ± 0.1	58.6 ± 5.8	68.3 ± 3.5
S_20OP	4.9 ± 2.7	43.7 ± 3.5	76.0 ± 1.4
S_40OP	4.9 ± 2.7	43.7 ± 3.5	69.3 ± 3.5
Sample	**TS (MPa)**	**ε_R (%)**	**E (MPa)**
S_0.1Ac	5.7 ± 0.2	78.4 ± 4.9	94.3 ± 12.3
S_0.1Ac_10OP	5.6 ± 0.2	66.1 ± 6.4	97.3 ± 5.7
S_0.1Ac_20OP	6.5 ± 0.2	53.3 ± 0.3	99.0 ± 6.5
S_0.1Ac_40OP	5.8 ± 0.2	50.9 ± 1.4	90.3 ± 9.0
Sample	**TS (MPa)**	**ε_R (%)**	**E (MPa)**
S_1Ac	4.5 ± 0.1	64.4 ± 7.7	57.0 ± 6.0
S_1Ac_10OP	4.7 ± 0.2	66.7 ± 3.0	61.6 ± 4.7
S_1Ac_20OP	3.6 ± 0.1	60.2 ± 4.3	35.3 ± 1.5
S_1Ac_40OP	3.6 ± 0.0	44.9 ± 5.8	37.6 ± 3.2
Sample	**TS (MPa)**	**ε_R (%)**	**E (MPa)**
S_0.1HCl	3.7 ± 0.2	30.8 ± 6.2	87.5 ± 5.0
S_0.1HCl_10OP	6.8 ± 0.5	28.4 ± 3.0	114.0 ± 0.0
S_0.1HCl_20OP	5.0 ± 0.5	31.3 ± 7.0	115.3 ± 8.4
S_0.1HCl_40OP	6.0 ± 0.4	48.7 ± 3.1	97.3 ± 8.0

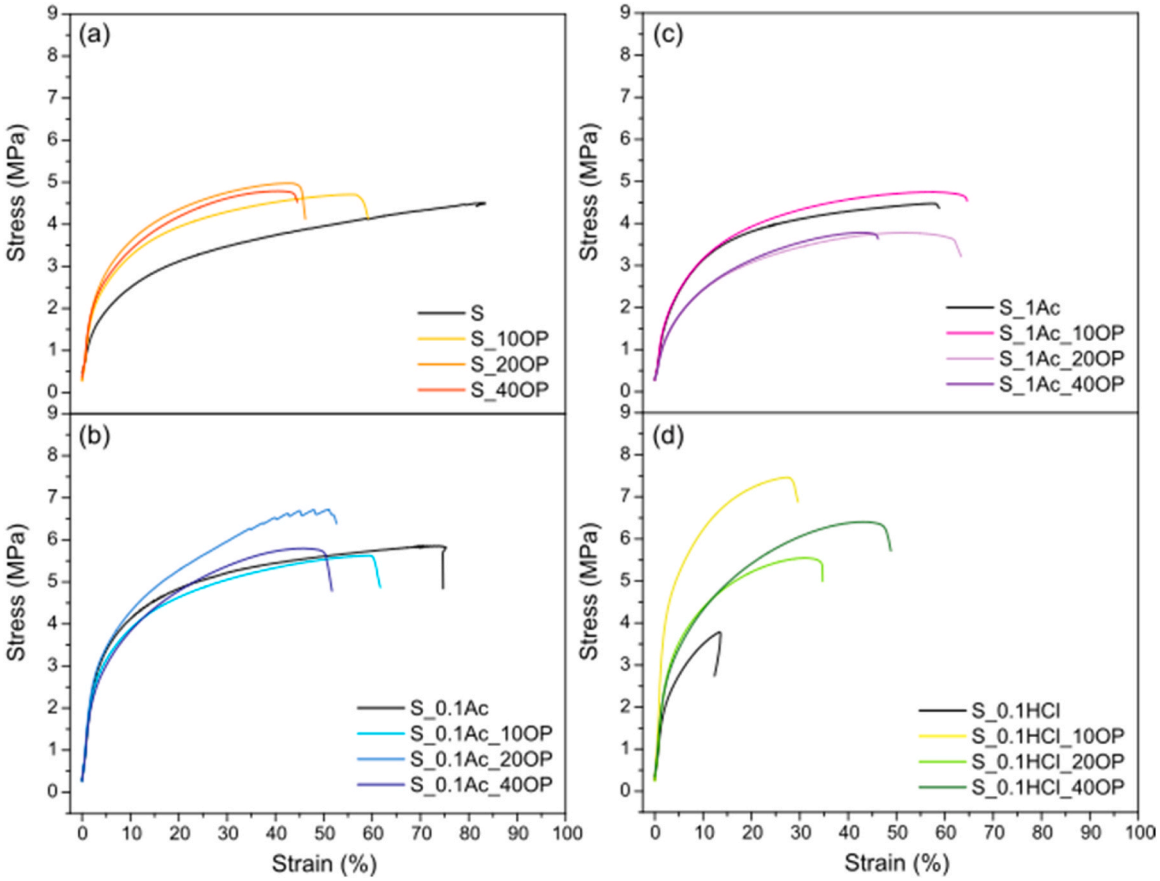

Fig. 7. (a) The stress-strain curves of S films containing 0, 10, 20, and 40 wt% of OP and treated with **(a)** water, **(b)** 0.1 M Ac, **(c)** 1 M Ac, and **(d)** 0.1 M HCl.

conditions, like 0.1 M Ac, showed better mechanical properties (i.e., higher modulus, elongation, and tensile strengths) with respect to the films treated with 1 M of acetic acid or 0.1 M of HCl to a greater extent. This could be related to the hydrolysis of starch chains under strong acid conditions (Utrilla-Coello et al., 2014; Wang and Copeland, 2015). However, contrary to the common undesirable stiffness effect of the filler observed in literature (Ali et al., 2019a; Quilez-Molina et al., 2022a; Wei et al., 2022), the addition of hydrolyzed OP could preserve the elastic behaviour of the starch in concentrations that reached the 40 wt%. For example, other films based on starch enriched with food-waste fillers added in lower concentrations like the cassava starch film loaded with 1.5 wt% of beetroot flour exhibited 1.6% of ε_R, and a TS of 0.59 MPa, while S_0.1Ac_20OP displayed 50% and 6.5 MPa of ε_R and TS, respectively (Otàlora Gonzàlez et al., 2020). In general, the reinforcement effect of a vegetable-biomass filler is commonly associated to the formation strong hydrogen-bond network with the matrix and their rigid nature, which restricts the mobility of the starch chains (Quilez-Molina et al., 2022a). As observed in infrared spectra of Fig. 2, weak acid conditions, like 0.1 M Ac, resulted into higher amount of hydroxyl groups, which can interact with the starch chains obtaining stronger mechanical response (Quilez-Molina et al., 2022a). The loss of mechanical strength of films processed with 1 M acetic acid was justified by the representative degradation of the biomass under these conditions.

Interestingly, in Fig. 7**(d),** the mechanical features of films treated with 0.1 M of HCl greatly improved with the addition of OP. The TS was almost the double, while ε_R increased in about 60%, for S-0.1HCl-40OP with respect to S-0.1HCl. The better mechanical performance with the increasing concentration of OP was strongly related with the esterification reaction between starch chains and organic acids derived from OP hydrolysis mentioned in the previous section (Fonseca-Florido et al., 2018; Morán et al., 2013). In bibliography, the esterification of starch is usually associated with a plasticizing effect due to the formation of bulky groups (Morán et al., 2013). Furthermore, the acid treatments improved the mechanical resistance of the films significantly as observed in those treated with 0.1 M Ac and HCl. For instance, the mechanical properties of S_0.1Ac_40OP are clearly better in terms of tensile strength, elongation at break and modulus than in the S_40_OP film, clearly showing the effectiveness of the acid treatment. Moreover, the properties of this film are also better than that of the initial starch in modulus and TS. Therefore, we can conclude that the approach followed in this research allows incorporating large amount of orange peel discard obtaining film with excellent mechanical performance.

As a result of their exceptional mechanical properties, some additional characteristics of the films containing 40 wt% of OP will be evaluated in the next sections.

3.7. Thermal properties of films

The influence of the acid treatment and addition of OP biomass in the starch films on the thermal stability will be discussed in this section. Fig. 8**(a)** displays the derivative thermogravimetric (DTG) curves of the thermal degradation of S films treated with different acids. The corresponding thermal degradation curves are displayed in Fig. S6 of Supporting information. The thermal decomposition profiles of samples reveal that the type of acid had a strong effect on the hydrolysis reaction. Generally, starch matrices degrade in three stages: at about 100ºC related to the loss of free water and glycerol molecules, and at about 300 ℃ and 330 ℃, assigned to the degradation of the glycerol-rich S fraction and the depolymerization and thermal decomposition of the S backbone respectively (Ilyas et al., 2018; Merino et al., 2019; Prachayawarakorn et al., 2011). In the thermograms of S samples treated with Ac these peaks are clearly distinguished. In the case of S_0.1Ac, the temperatures of maximum-mass loss rates are slightly displaced towards lower temperatures, evidencing the loss of the thermal resistance. On the other hand, the first degradation peak is barely distinguished in the S_1Ac sample, displaying a single degradation stage. This suggested that this reaction medium improved the mixing between glycerol and starch resulted in a more homogeneous matrix (Collazo-Bigliardi et al., 2019; Merino et al., 2019). The thermogram of S_0.1HCl displayed a new

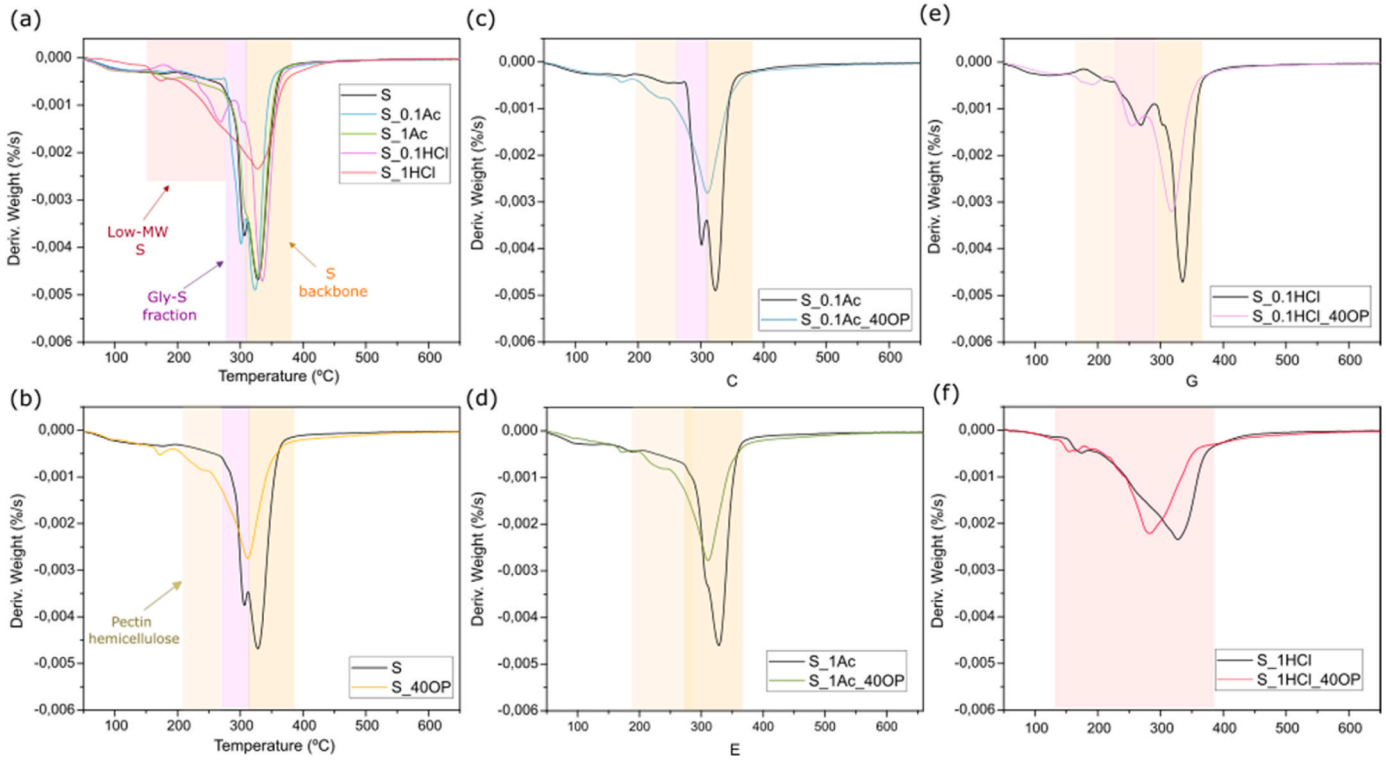

Fig. 8. (a) The derivative weight curves of starch samples treated under different acid conditions. The DTG curves and derivative thermal curves of the starch samples and OP-starch composites treated with: **(b)** water, **(c)** 0.1 M Ac, **(d)** 1 M Ac, **(e)** 0.1 HCl, and **(f)** 1 M HCl. Starch films without filler are presented in black.

degradation step at lower temperatures (268 ℃), indicating the presence of low-molecular weight (MW) starch that degrade at an earlier stage (Zuo et al., 2014). The decomposition of S_1HCl sample undergoes in a single step at low temperatures showing the high degradation state of the starch matrix, in concordance with the abovementioned results. The thermal data collected in Table S2 reveals that the thermal stability of the polymer backbone, which refers to the T_{max} of 2nd decomposition peak, increased with the acid treatment strength (0.1 M Ac < 1 M Ac < 0.1 M HCl). This enhancement in the thermal properties can be associated with the increase of the starch crystallinity, which is usually companied by a higher density of the polymer entanglements (Li et al., 2018), see Fig. 6**(a).**

The derivative curves for S films enriched with a 40 wt% of OP are displayed in Fig. 8**(b-f),** while the TG curves are represented in Fig. S6 **(b-e)** of Supporting information. All composites displayed degradation peaks characteristic to each component (vegetable additive and starch matrix). Most of S-OP composites exhibited a first peak of mass loss in a range 170–230 ℃ assigned to the degradation of the hemicellulose and pectin fraction of the biomass, see the TGA of OP in Fig. 2**(c)** (Açıkalın, n.d.). Interestingly, the thermal degradation of the starch biopolymer fraction in the S-OP composites occurred in a single step, at around 310 ℃, against the two degradation steps observed in the neat S film (about 300 ℃ and 330 ℃) (Fig. 8**(a)**). This indicated that the addition of OP enhanced the thermal stability and the homogenization of the S (Collazo-Bigliardi et al., 2019; Merino et al., 2019). The decomposition curves of samples treated with HCl, in all concentrations (0.1 M, 1 M), exhibited the degradation stages associated to the LMW products resulted from the hydrolysis of starch. However, only S_0.1HCl_40OP displayed the thermal curve of the degradation of hemicellulose and pectin (highlighted in brown). The lack of this curve in the S_1HCl_40OP sample indicated that these components were degraded during the hydrolysis of the OP with 1 M HCl.

The thermal data collected in Table S2 indicated that an overall decrement of thermal resistance (∼10ºC) occurred in films with the addition of orange peel, attributed to the lower thermal resistance of the OP components (onset degradation temperature of pectin and hemicellulose below 200ºC) (Açıkalın, n.d.; Merino et al., 2021). The thermal stability of the present composites overcame the values obtained other corn starch-based films made up of natural fibers, such as those containing rice or coffe husk in 20–40 wt%, or corn husk fiber (4–8 wt%), which displayed a Tmax of about 295 ℃ and 280 ℃, respectively (Collazo-Bigliardi et al., 2019; Ibrahim et al., 2019).

3.8. Water resistance properties

The weak moisture resistance has been considered the main drawback for the application of starch-based materials (Otàlora Gonzàlez et al., 2020). The effect of the acid exposure and the addition of OP filler in 40 wt% on the moisture properties will be evaluated in the next paragraphs. Fig. 9**(a)** shows that the exposure to acid conditions of S leads to a slight increase of moisture content (MC), of about 5.5%, for films treated with Ac. For S_0.1HCl the MC increased in ∼15%, associated to the partial degradation of the S matrix when exposure to the stronger acid condition (Martins and Martins, 2021). The incorporation of 40 wt% OP, rich in polar groups resulted into the increased of MC for S films treated at less moderate conditions, water and 0.1 M Ac, with an increase of 9% and 3% with respect to films made for only starch. The opposite tendency was observed in S_1Ac and S_0.1HCl films, likely due to the interaction between the OP components and the partially hydrolyzed starch matrix, which reduce the interaction of -OH groups of starch with moisture leading into an increase the water resistance (Chhatariya et al., 2022; Martins and Martins, 2021; Ribeiro Sanches et al., 2021). Moreover, the formation of hydrophic humins as product of the hydrolysis reaction with HCl may enhance the water resistance (Sangregorio et al., 2019). The MC values of films with 40 wt% of OP ranged from 6.1% to 6.5%, for S_0.1HCl_40OP and S_40OP, respectively, similar to other starch films loaded with lignocellulosic fillers (Ribeiro Sanches et al., 2021).

The water vapor sorption kinetics curves of starch films and composite films loaded with 40 wt% of OP at 75% relative humidity (RH) are exhibited in Fig. S7**(a)**. This graphic shows that the water sorption occurred quickly during the first 24 h, while the equilibrium condition was reached after 4 days in all films, obtaining final moisture adsorption values ranging from 23.5% to 25%. However, other starch-based films exposed to the same humidity conditions, such as citric acid-modified porous starch reported by Qian et al. (2011) reached the equilibrium after 6 days, with MAd varying from 32.5% to 45%. Another example are potato starch films containing 30 wt% of agar, which did not attain the equilibrium after being storaged for more than 4 days (Wu et al., 2009). Fig. 9**(b)** displays the values of moisture adsorption (MAd) at equilibrium. In the plotted data can be observed that orange peel strengthened the water resistance by reducing the amount of moisture absorbed. The upgrading effect of orange peel was enhanced in samples treated with acid, especially with HCl. Indeed, S_0.1HCl film could not be measured because it leaks water, hampering the measuring and compromising the reliability of the results. However, this effect was not observed in the analogue sample containing 40 wt% of OP, S_0.1HCl_40OP. This effect was clearly observed in the MAd values of

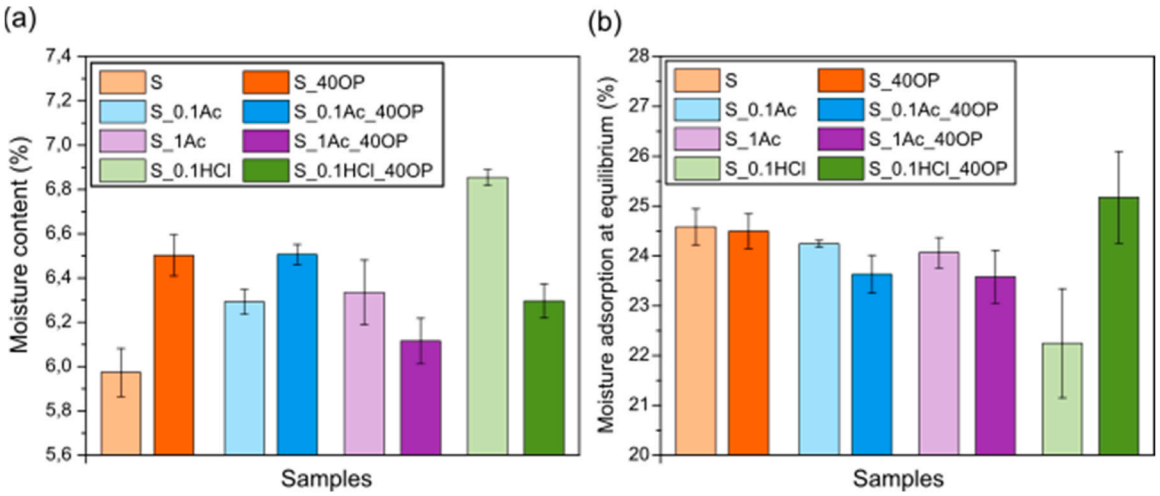

Fig. 9. (a) The MC, and **(b)** Moisture adsorption at equilibrium conditions of unfilled and OP-filled starch composites.

films collected during the first 24 h, reported in Fig. S7**(b)**.

The solubility values are displayed in Fig. S8 of Supporting information because the results obtained were barely remarkable. The graph indicated that the acid treatment did not have an important influence in the solubility properties of films, maintaining a constant value of ~30%, similar to other starch composites reported in the literature (Zhang et al., 2011). As expected, the solubility increased with the addition of the filler up to ~37% due to the presence of water-soluble molecules present in the orange peel, such as pectin, which concentration ranges 30–45% (Chhatariya et al., 2022; Merino et al., 2021). The most relevant result was obtained in S_0.1HCl_40OP films. Herein is proven that the incorporation of vegetable biomass strengthened the poor solubility of S_0.1HCl films, maintaining its integrity after the water immersion, see Fig. S8**(b)**. The esterification of starch with the organic acids resulted from the acid hydrolysis observed in the infrared section could justify this result (Chung and Lai, 2007; Martins and Martins, 2021). Interestingly, the best water solubility value obtained in films 100% based on orange peel was 46%, while the highest solubility in OP-starch composites was ~37% (Quilez-Molina et al., 2022b).

4. Conclusions

The food waste orange peel demonstrated to have excellent features to be used as an additive for starch matrices, allowing loads up to 40 wt % of OP, and preserving the good films capability and mechanical features of the starch. Even so, it was demonstrated that the compatibility of both components and final properties can be improved by hydrolyzing the orange peel before the gelatinization. Overall, the acid conditions used showed to be critical to define the final properties of the materials, especially due to high sensitivity of starch matrix to hydrolyze. Results showed that weak organic acid, like acetic acid, did not promote important chemical changes in both biomass and starch matrix. Meanwhile, the inorganic acid HCl conducted the hydrolysis of starch chains, compromising the film formation capability and the final properties of the materials. However, these latter features could be improved in combination with hydrolyzed biomass. This is because HCl triggered oxidation and condensation reactions of the orange peel that resulted into high-value products (i.e., humic substances and organic acids), which interacted with starch by esterification improving the compatibility and enhancing the mechanical and moisture resistance properties. Therefore, these chemical reactions provided the possibility to tune the characteristics of films based on food-waste obtaining sustainable composites with better properties than many others found in the state of the art (Merino et al., 2022; Quilez-Molina et al., 2022b).

Among them, S-OP film processed with 1 M Ac exhibited the best overall performance, displaying superior moisture resistance but also keeping the excellent mechanical features of the starch matrix. To conclude, we demonstrated a simple and scalable method to tune and upgrade the final features of biocomposites with a content of agri-food discard of up to 40 wt%. A similar effect is expected from the acid hydrolysis on the filler and starch to a great extent, considering that the degree of hydrolysis could slightly vary with the chemical features of the starch (degree of crystallinity, ratio amylopectin/amylose) (Singh and Ali, 2008). But overall, it can be assumed that the results obtained in this work could be largely extrapolated to other starch composites containing fillers rich in pectin, such as orange peel, to enhance the performance of these promising materials.

CRediT authorship contribution statement

The experimental work was carried out by A.Q., L.O., and C.A.; data analysis was performed by A.Q.; the article was written by A.Q.; the article was reviewed by L.O., A.L., and M.R.; the article was supervised by A.Q., L.O., A.L., and M.R. All authors have read and agreed to publish the manuscript.

Declaration of Competing Interest

The authors declare that they have no known competing financial interests or personal relationships that could have appeared to influence the work reported in this paper.

Data Availability

No data was used for the research described in the article.

Acknowledgements

Financial assistance from Ministerio de Ciencia, Innovación y Universidades (MCIU) (Spain) (RTI2018 - 098749-B-I00, PID2021-127108OB-I00, TED2021-130965B-I00 and PDC2022-133391-I00), Regional Government of Castilla y León and the EU-FEDER program (CLU-2019-04 and VA202P20) are gratefully acknowledged. This work was supported by the Regional Government of Castilla y León (Junta de Castilla y León), and by the Ministry of Science and Innovation MICIN and the European Union NextGenerationEU / PRTR. Authors want to thank the Instituto Tecnológico Agrario de Castilla y León (ITACYL) for developing the chemical analysis of starch within the project BIOPAGRO (RTC2019-006989-5), funded by the Ministry of Science and Innovation and the AEI (Spanish Government) under the funding program RETOS COLABORACION. Finally, the Spanish Ministry of Universities and the Next Generation EU-Recovery are also acknowledged for funding the post-doctoral grant “Margarita Salas” (CONVREC-2022-63) of A. Q.

Appendix A. Supporting information

Supplementary data associated with this article can be found in the online version at doi:10.1016/j.indcrop.2023.117407.

References

Abdillah, A.A., Charles, A.L., 2021. Characterization of a natural biodegradable edible film obtained from arrowroot starch and iota-carrageenan and application in food packaging. Int. J. Biol. Macromol. 191, 618–626. https://doi.org/10.1016/j.ijbiomac.2021.09.141.

Abe, M.M., Martins, J.R., Sanvezzo, P.B., Macedo, J.V., Branciforti, M.C., Halley, P., Botaro, V.R., Brienzo, M., 2021. Advantages and disadvantages of bioplastics production from starch and lignocellulosic components. Polymers. https://doi.org/10.3390/polym13152484.

Açıkalın, K., n.d. Evaluation of orange and potato peels as an energy source: a comprehensive study on their pyrolysis characteristics and kinetics. https://doi.org/10.1007/s13399–021-01387-z/Published.

Ali, A., Ali, S., Yu, L., Liu, H., Khalid, S., Hussain, A., Qayum, M.M.N., Ying, C., 2019a. Preparation and characterization of starch-based composite films reinforced by apricot and walnut shells. J. Appl. Polym. Sci. 136. https://doi.org/10.1002/app.47978.

Ali, A., Chen, Y., Liu, H., Yu, L., Baloch, Z., Khalid, S., Zhu, J., Chen, L., 2019b. Starch-based antimicrobial films functionalized by pomegranate peel. Int. J. Biol. Macromol. 129, 1120–1126. https://doi.org/10.1016/j.ijbiomac.2018.09.068.

Altayan, M.M., al Darouich, T., Karabet, F., 2017. On the plasticization process of potato starch: preparation and characterization. Food Biophys. 12, 397–403. https://doi.org/10.1007/s11483-017-9495-2.

Area, M.R., Rico, M., Montero, B., Barral, L., Bouza, R., López, J., Ramírez, C., 2019. Corn starch plasticized with isosorbide and filled with microcrystalline cellulose: Processing and characterization. Carbohydr. Polym. 206, 726–733. https://doi.org/10.1016/j.carbpol.2018.11.055.

Benito-González, I., López-Rubio, A., Martínez-Sanz, M., 2019. High-performance starch biocomposites with celullose from waste biomass: Film properties and retrogradation behaviour. Carbohydr. Polym. 216, 180–188. https://doi.org/10.1016/j.carbpol.2019.04.030.

Bizzani, M., Flores, D.W.M., Colnago, L.A., Ferreira, M.D., 2017. Non-invasive spectroscopic methods to estimate orange firmness, peel thickness, and total pectin content. Microchem. J. 133, 168–174. https://doi.org/10.1016/j.microc.2017.03.039.

Bodirlau, R., Teaca, C.A., Spiridon, I., 2013. Influence of natural fillers on the properties of starch-based biocomposite films. Compos B Eng. 44, 575–583. https://doi.org/10.1016/j.compositesb.2012.02.039.

Boluda-Aguilar, M., López-Gómez, A., 2013. Production of bioethanol by fermentation of lemon (Citrus limon L.) peel wastes pretreated with steam explosion. Ind. Crop. Prod. 41, 188–197. https://doi.org/10.1016/j.indcrop.2012.04.031.

Boukroufa, M., Boutekedjiret, C., Petigny, L., Rakotomanomana, N., Chemat, F., 2015. Bio-refinery of orange peels waste: A new concept based on integrated green and solvent free extraction processes using ultrasound and microwave techniques to obtain essential oil, polyphenols and pectin. Ultrason. Sonochem. 24, 72–79. https://doi.org/10.1016/j.ultsonch.2014.11.015.

Bruni, G.P., de Oliveira, J.P., Fonseca, L.M., da Silva, F.T., Dias, A.R.G., da Rosa Zavareze, E., 2020. Biocomposite films based on phosphorylated wheat starch and cellulose nanocrystals from rice, oat, and eucalyptus husks. Starch-Stärke 72, 1900051. https://doi.org/10.1002/star.201900051.

Campagnolo, L., Morselli, D., Magrì, D., Scarpellini, A., Demirci, C., Colombo, M., Athanassiou, A., Fragouli, D., 2019. Silk fibroin/orange peel foam: an efficient biocomposite for water remediation. Adv. Sustain. Syst. 3. https://doi.org/10.1002/adsu.201800097.

Chakraborty, I., N, P., Mal, S.S., Paul, U.C., Rahman, M.H., Mazumder, N., 2022. An insight into the gelatinization properties influencing the modified starches used in food industry: a review. Food Bioprocess Technol. https://doi.org/10.1007/s11947-022-02761-z.

Chang, Y.H., Lin, J.H., Chang, S.Y., 2006. Physicochemical properties of waxy and normal corn starches treated in different anhydrous alcohols with hydrochloric acid. Food Hydrocoll. 332–339. https://doi.org/10.1016/j.foodhyd.2005.02.024.

Chen, Y., Liu, C., Chang, P.R., Cao, X., Anderson, D.P., 2009. Bionanocomposites based on pea starch and cellulose nanowhiskers hydrolyzed from pea hull fibre: Effect of hydrolysis time. Carbohydr. Polym. 76, 607–615. https://doi.org/10.1016/j.carbpol.2008.11.030.

Chhatariya, H.F., Srinivasan, S., Choudhary, P.M., Begum, S.S., 2022. Corn starch biofilm reinforced with orange peel powder: Characterization of physicochemical and mechanical properties. Mater. Today Proc. 59, 884–892. https://doi.org/10.1016/j.matpr.2022.01.339.

Chung, Y.L., Lai, H.M., 2007. Properties of cast films made of HCI-methanol modified corn starch. Starch/Staerke 59, 583–592. https://doi.org/10.1002/star.200700639.

Collazo-Bigliardi, S., Ortega-Toro, R., Chiralt Boix, A., 2018. Isolation and characterisation of microcrystalline cellulose and cellulose nanocrystals from coffee husk and comparative study with rice husk. Carbohydr. Polym. 191, 205–215. https://doi.org/10.1016/j.carbpol.2018.03.022.

Collazo-Bigliardi, S., Ortega-Toro, R., Chiralt, A., 2019. Improving properties of thermoplastic starch films by incorporating active extracts and cellulose fibres isolated from rice or coffee husk. Food Package Shelf Life 22, 100383. https://doi.org/10.1016/j.fpsl.2019.100383.

Dwyer, J., Starrenburg, D., Tait, S., Barr, K., Batstone, D.J., Lant, P., 2008. Decreasing activated sludge thermal hydrolysis temperature reduces product colour, without decreasing degradability. Water Res. 42, 4699–4709. https://doi.org/10.1016/j.watres.2008.08.019.

Espinosa, E., Rincón, E., Morcillo-Martín, R., Rabasco-Vílchez, L., Rodríguez, A., 2022. Orange peel waste biorefinery in multi-component cascade approach: Polyphenolic compounds and nanocellulose for food packaging. Ind. Crop. Prod. 187. https://doi.org/10.1016/j.indcrop.2022.115413.

Fitch-Vargas, P.R., Camacho-Hernández, I.L., Rodríguez-González, F.J., Martínez-Bustos, F., Calderón-Castro, A., Zazueta-Morales, J., de, J., Aguilar-Palazuelos, E., 2023. Effect of compounding and plastic processing methods on the development of bioplastics based on acetylated starch reinforced with sugarcane bagasse cellulose fibers. Ind. Crop. Prod. 192. https://doi.org/10.1016/j.indcrop.2022.116084.

Fonseca-Florido, H.A., Vázquez-García, H.G., Méndez-Montealvo, G., Basilio-Cortés, U. A., Navarro-Cortés, R., Rodríguez-Marín, M.L., Castro-Rosas, J., Gómez-Aldapa, C.A., 2018. Effect of acid hydrolysis and OSA esterification of waxy cassava starch on emulsifying properties in Pickering-type emulsions. LWT 91, 258–264. https://doi.org/10.1016/j.lwt.2018.01.057.

Gallo, M., Arrighi, G., Moreschi, L., Del Borghi, A., Athanassiou, A., Perotto, G., 2022. Life cycle assessment of a circular economy process for tray production via water-based upcycling of vegetable waste. ACS Sustain. Chem. Eng. 10, 13936–13944. https://doi.org/10.1021/acssuschemeng.2c02942.

Gebresas, G.A., Szabó, T., Marossy, K., 2023. A comparative study of carboxylic acids on the cross-linking potential of corn starch films. J. Mol. Struct. 1277. https://doi.org/10.1016/j.molstruc.2022.134886.

Homthawornchoo, W., Han, J., Kaewprachu, P., Romruen, O., Rawdkuen, S., 2022. Green tea extract enrichment: mechanical and physicochemical properties improvement of rice starch-pectin composite film. Polymers 14. https://doi.org/10.3390/polym14132696.

Ibrahim, M.I.J., Sapuan, S.M., Zainudin, E.S., Zuhri, M.Y.M., 2019. Potential of using multiscale corn husk fiber as reinforcing filler in cornstarch-based biocomposites. Int. J. Biol. Macromol. 139, 596–604. https://doi.org/10.1016/j.ijbiomac.2019.08.015.

Ilyas, R.A., Sapuan, S.M., Ishak, M.R., Zainudin, E.S., 2018. Development and characterization of sugar palm nanocrystalline cellulose reinforced sugar palm starch bionanocomposites. Carbohydr. Polym. 202, 186–202. https://doi.org/10.1016/j.carbpol.2018.09.002.

Islam, M.N., Jiang, Y., 2022. 3D printable sustainable composites with thermally tunable properties entirely from corn-based products. ACS Sustain. Chem. Eng. 10, 7818–7824. https://doi.org/10.1021/acssuschemeng.2c01806.

Ismail, I., Osman, A.F., Leong Ping, T., 2019. Effects of ultrasonication process on crystallinity and tear strength of thermoplastic starch/cellulose biocomposites. In: IOP Conference Series: Materials Science and Engineering. IOP Publishing Ltd. https://doi.org/10.1088/1757-899X/701/1/012045.

Ivanovska, A., Gajić, I.S., Lađarević, J., Milošević, M., Savić, I., Mihajlovski, K., Kostić, M., 2022. Sustainable dyeing and functionalization of different fibers using orange peel extract's. Antioxidants 11. https://doi.org/10.3390/antiox11102059.

Karma, V., Gupta, A.D., Yadav, D.K., Singh, A.A., Verma, M., Singh, H., 2022. Recent developments in starch modification by organic acids: a review. Starch/Staerke. https://doi.org/10.1002/star.202200025.

Khorasani, A.C., Shojaosadati, S.A., 2017. Pectin-non-starch nanofibers biocomposites as novel gastrointestinal-resistant prebiotics. Int. J. Biol. Macromol. 94, 131–144. https://doi.org/10.1016/j.ijbiomac.2016.10.011.

Kumar, A., Singh Negi, Y., Choudhary, V., Kant Bhardwaj, N., 2020. Characterization of cellulose nanocrystals produced by acid-hydrolysis from sugarcane bagasse as agro-waste. J. Mater. Phys. Chem. 2, 1–8. https://doi.org/10.12691/jmpc-2-1-1.

Kurita, O., Fujiwara, T., Yamazaki, E., 2008. Characterization of the pectin extracted from citrus peel in the presence of citric acid. Carbohydr. Polym. 74, 725–730. https://doi.org/10.1016/j.carbpol.2008.04.033.

Li, M., Tian, X., Jin, R., Li, D., 2018. Preparation and characterization of nanocomposite films containing starch and cellulose nanofibers. Ind. Crop. Prod. 123, 654–660. https://doi.org/10.1016/j.indcrop.2018.07.043.

Li, M., Pu, Y., Thomas, V.M., Yoo, C.G., Ozcan, S., Deng, Y., Nelson, K., Ragauskas, A.J., 2020. Recent advancements of plant-based natural fiber–reinforced composites and their applications. Compos. B Eng. https://doi.org/10.1016/j.compositesb.2020.108254.

Liu, L., Li, Z., Hou, W., Shen, H., 2018. Direct conversion of lignocellulose to levulinic acid catalyzed by ionic liquid. Carbohydr. Polym. 181, 778–784. https://doi.org/10.1016/j.carbpol.2017.11.078.

Lopez-Gil, A., Rodriguez-Perez, M.A., De Saja, J.A., Bellucci, F.S., Ardanuy, M., 2014. Strategies to improve the mechanical properties of starch-based materials: plasticization and natural fibers reinforcement. Polimeros 24, 36–42. https://doi.org/10.4322/polimeros.2014.054.

Ma, X., Chang, P.R., Yu, J., Stumborg, M., 2009. Properties of biodegradable citric acid-modified granular starch/thermoplastic pea starch composites. Carbohydr. Polym. 75, 1–8. https://doi.org/10.1016/j.carbpol.2008.05.020.

Martins, P.C., Martins, V.G., 2021. Effect of rice starch hydrolysis and esterification processes on the physicochemical properties of biodegradable films. Starch/Staerke 73. https://doi.org/10.1002/star.202100022.

Ma, S., Yan, Y., He, C., Li, Z., Tang, X., Sperry, J., Sun, Y., Lin, L., Zeng, X., 2022. Production of biomass-based composite from reed pretreated by ball-milling combined with p-toluenesulfonic acid. Ind. Crop. Prod. 180. https://doi.org/10.1016/j.indcrop.2022.114712.

Menzel, C., Olsson, E., Plivelic, T.S., Andersson, R., Johansson, C., Kuktaite, R., Järnström, L., Koch, K., 2013. Molecular structure of citric acid cross-linked starch films. Carbohydr. Polym. 96, 270–276. https://doi.org/10.1016/j.carbpol.2013.03.044.

Merino, D., Gutiérrez, T.J., Mansilla, A.Y., Casalongué, C.A., Alvarez, V.A., 2018. Critical evaluation of starch-based antibacterial nanocomposites as agricultural mulch films: study on their interactions with water and light. ACS Sustain Chem. Eng. 6, 15662–15672. https://doi.org/10.1021/acssuschemeng.8b04162.

Merino, D., Gutiérrez, T.J., Alvarez, V.A., 2019. Structural and thermal properties of agricultural mulch films based on native and oxidized corn starch nanocomposites. Starch/Staerke 71. https://doi.org/10.1002/star.201800341.

Merino, D., Simonutti, R., Perotto, G., Athanassiou, A., 2021. Direct transformation of industrial vegetable waste into bioplastic composites intended for agricultural mulch films. Green Chem. 23, 5956–5971. https://doi.org/10.1039/d1gc01316e.

Merino, D., Quilez-Molina, A.I., Perotto, G., Bassani, A., Spigno, G., Athanassiou, A., 2022. A second life for fruit and vegetable waste: a review on bioplastic films and coatings for potential food protection applications. Green Chem. https://doi.org/10.1039/D1GC03904K.

Mohamad, N., Abd-Talib, N., Kelly Yong, T.L., 2020. Furfural production from oil palm frond (OPF) under subcritical ethanol conditions. In: Materials Today: Proceedings. Elsevier Ltd, pp. 116–121. https://doi.org/10.1016/j.matpr.2020.01.256.

Morán, J.I., Vázquez, A., Cyras, V.P., 2013. Bio-nanocomposites based on derivatized potato starch and cellulose, preparation and characterization. J. Mater. Sci. 48, 7196–7203. https://doi.org/10.1007/s10853-013-7536-x.

Müller, P., Renner, K., Móczó, J., Fekete, E., Pukánszky, B., 2014. Thermoplastic starch/wood composites: Interfacial interactions and functional properties. Carbohydr. Polym. 102, 821–829. https://doi.org/10.1016/j.carbpol.2013.10.083.

Osman, A.F., Ashafee, A.M.T.L., Adnan, S.A., Alakrach, A., 2020. Influence of hybrid cellulose/bentonite fillers on structure, ambient, and low temperature tensile properties of thermoplastic starch composites. Polym. Eng. Sci. 60, 810–822. https://doi.org/10.1002/pen.25340.

Otàlora Gonzàlez, C.M., Flores, S.K., Basanta, M.F., Gerschenson, L.N., 2020. Effect of beetroot (Beta vulgaris L. var conditiva) fiber filler and corona treatment on cassava starch films properties. Food Packag Shelf Life 26. https://doi.org/10.1016/j.fpsl.2020.100605.

Palanisamy, C.P., Cui, B., Zhang, H., Jayaraman, S., Muthukaliannan, G.K., 2020. A comprehensive review on corn starch-based nanomaterials: Properties, simulations, and applications. Polymers. https://doi.org/10.3390/POLYM12092161.

Perotto, G., Ceseracciu, L., Simonutti, R., Paul, U.C., Guzman-Puyol, S., Tran, T.N., Bayer, I.S., Athanassiou, A., 2018. Bioplastics from vegetable waste: Via an eco-friendly water-based process. Green Chem. 20, 894–902. https://doi.org/10.1039/c7gc03368k.

Pin, J.M., Guigo, N., Mija, A., Vincent, L., Sbirrazzuoli, N., van der Waal, J.C., de Jong, E., 2014. Valorization of biorefinery side-stream products: combination of humins with polyfurfuryl alcohol for composite elaboration. ACS Sustain. Chem. Eng. 2, 2182–2190. https://doi.org/10.1021/sc5003769.

Prachayawarakorn, J., Ruttanabus, P., Boonsom, P., 2011. Effect of cotton fiber contents and lengths on properties of thermoplastic starch composites prepared from rice and

waxy rice starches. J. Polym. Environ. 19, 274–282. https://doi.org/10.1007/s10924-010-0273-1.
Qian, D., Chang, P.R., Ma, X., 2011. Preparation of controllable porous starch with different starch concentrations by the single or dual freezing process. Carbohydr. Polym. 86, 1181–1186. https://doi.org/10.1016/j.carbpol.2011.06.012.
Quilez-Molina, A.I., Heredia-Guerrero, J.A., Armirotti, A., Paul, U.C., Athanassiou, A., Bayer, I.S., 2020. Comparison of physicochemical, mechanical and antioxidant properties of polyvinyl alcohol films containing green tealeaves waste extracts and discarded balsamic vinegar. Food Package Shelf Life 23. https://doi.org/10.1016/j.fpsl.2019.100445.
Quilez-Molina, A.I., Chandra Paul, U., Merino, D., Athanassiou, A., 2022a. Composites of thermoplastic starch and lignin-rich agricultural waste for the packaging of fatty foods. ACS Sustain Chem. Eng. https://doi.org/10.1021/acssuschemeng.2c04326.
Quilez-Molina, A.I., Mazzon, G., Athanassiou, A., Perotto, G., 2022b. A novel approach to fabricate edible and heat sealable bio-based films from vegetable biomass rich in pectin. Mater. Today Commun., 103871 https://doi.org/10.1016/j.mtcomm.2022.103871.
Reinaldo, J.S., Milfont, C.H.R., Gomes, F.P.C., Mattos, A.L.A., Medeiros, F.G.M., Lopes, P.F.N., Matsui, K.N., Ito, E.N., 2021. Influence of grape and acerola residues on the antioxidant, physicochemical and mechanical properties of cassava starch biocomposites. Polym. Test. 93, 107015.
Ribeiro Sanches, M.A., Camelo-Silva, C., Tussolini, L., Tussolini, M., Zambiazi, R.C., Becker Pertuzatti, P., 2021. Development, characterization and optimization of biopolymers films based on starch and flour from jabuticaba (Myrciaria cauliflora) peel. Food Chem. 343. https://doi.org/10.1016/j.foodchem.2020.128430.
Salasinska, K., Barczewski, M., Górny, R., Kloziński, A., 2018. Evaluation of highly filled epoxy composites modified with walnut shell waste filler. Polym. Bull. 75, 2511–2528. https://doi.org/10.1007/s00289-017-2163-3.
Sangregorio, A., Guigo, N., van der Waal, J.C., Sbirrazzuoli, N., 2019. All 'green' composites comprising flax fibres and humins' resins. Compos Sci. Technol. 171, 70–77. https://doi.org/10.1016/j.compscitech.2018.12.008.
Sani, I.K., Geshlaghi, S.P., Pirsa, S., Asdagh, A., 2021. Composite film based on potato starch/apple peel pectin/ZrO2 nanoparticles/ microencapsulated Zataria multiflora essential oil; investigation of physicochemical properties and use in quail meat packaging. Food Hydrocoll. 117. https://doi.org/10.1016/j.foodhyd.2021.106719.
Sila, D.N., van Buggenhout, S., Duvetter, T., Fraeye, I., de Roeck, A., van Loey, A., Hendrickx, M., 2009. Pectins in processed fruits and vegetables: Part II - Structure-function relationships. Compr. Rev. Food Sci. Food Saf. https://doi.org/10.1111/j.1541-4337.2009.00071.x.
Singh, V., Ali, S.Z., 2008. Properties of starches modified by different acids. Int. J. Food Prop. 11, 495–507. https://doi.org/10.1080/10942910802083774.
Strawhecker, K.E., Kumar, S.K., Douglas, J.F., Karim, A., 2001. The critical role of solvent evaporation on the roughness of spin-cast polymer films [1]. Macromolecules. https://doi.org/10.1021/ma001440d.
Świątek, K., Gaag, S., Klier, A., Kruse, A., Sauer, J., Steinbach, D., 2020. Acid hydrolysis of lignocellulosic biomass: Sugars and furfurals formation. Catalysts 10. https://doi.org/10.3390/catal10040437.
Szymanska-Chargot, M., Zdunek, A., 2013. Use of FT-IR spectra and PCA to the bulk characterization of cell wall residues of fruits and vegetables along a fraction process. Food Biophys. 8, 29–42. https://doi.org/10.1007/s11483-012-9279-7.
Teacă, C.A., Bodîrlău, R., Spiridon, I., 2013. Effect of cellulose reinforcement on the properties of organic acid modified starch microparticles/plasticized starch bio-composite films. Carbohydr. Polym. 307–315. https://doi.org/10.1016/j.carbpol.2012.10.020.
Terzioğlu, P., Güney, F., Parın, F.N., Şen, İ., Tuna, S., 2021. Biowaste orange peel incorporated chitosan/polyvinyl alcohol composite films for food packaging applications. Food Package Shelf Life 30. https://doi.org/10.1016/j.fpsl.2021.100742.
Tian, Y., Zhou, M., Luo, T., Zhu, P.X., Cheng, F., Zhang, Y., Lin, Y., 2022. A comparative investigation of gelatinized and regenerated starch composites reinforced by microfibrillated cellulose. Food Chem. 373. https://doi.org/10.1016/j.foodchem.2021.131470.
Toro-Márquez, L.A., Merino, D., Gutiérrez, T.J., 2018. Bionanocomposite films prepared from corn starch with and without nanopackaged Jamaica (Hibiscus sabdariffa) flower extract. Food Bioprocess Technol. 11, 1955–1973. https://doi.org/10.1007/s11947-018-2160-z.
de la Torre, I., Martin-Dominguez, V., Acedos, M.G., Esteban, J., Santos, V.E., Ladero, M., 2019. Utilisation/upgrading of orange peel waste from a biological biorefinery perspective. Appl. Microbiol. Biotechnol. https://doi.org/10.1007/s00253-019-09929-2.
Trache, D., Hussin, M.H., Haafiz, M.K.M., Thakur, V.K., 2017. Recent progress in cellulose nanocrystals: Sources and production. Nanoscale. https://doi.org/10.1039/c6nr09494e.
Utrilla-Coello, R.G., Hernández-Jaimes, C., Carrillo-Navas, H., González, F., Rodríguez, E., Bello-Pérez, L.A., Vernon-Carter, E.J., Alvarez-Ramírez, J., 2014. Acid hydrolysis of native corn starch: Morphology, crystallinity, rheological and thermal properties. Carbohydr. Polym. 103, 596–602. https://doi.org/10.1016/j.carbpol.2014.01.046.
Valdivieso Ramirez, C.S., Sanchez Gallego, J.E., Gänzle, M., Temelli, F., Saldaña, M.D.A., 2021. Carboxylic acid-catalysed hydrolysis of polygalacturonic acid in subcritical water media. J. Supercrit. Fluids 169. https://doi.org/10.1016/j.supflu.2020.105103.
Wan, Y.Z., Luo, H., He, F., Liang, H., Huang, Y., Li, X.L., 2009. Mechanical, moisture absorption, and biodegradation behaviours of bacterial cellulose fibre-reinforced starch biocomposites. Compos. Sci. Technol. 69, 1212–1217. https://doi.org/10.1016/j.compscitech.2009.02.024.
Wang, S., Copeland, L., 2015. Effect of acid hydrolysis on starch structure and functionality: a review. Crit. Rev. Food Sci. Nutr. 55, 1081–1097. https://doi.org/10.1080/10408398.2012.684551.
Warren, F.J., Gidley, M.J., Flanagan, B.M., 2016. Infrared spectroscopy as a tool to characterise starch ordered structure - a joint FTIR-ATR NMR, XRD and DSC study. Carbohydr. Polym. 139, 35–42. https://doi.org/10.1016/j.carbpol.2015.11.066.
Wei, X., Tang, J., Tao, H., Gao, W., Guo, L., Cui, B., Liu, P., Lu, L., Wu, Z., Fang, Y., Zhao, M., Yang, N., Huang, Q., 2022. Correlation between interfacial adhesion and functional properties of corn stalk cellulose-reinforced corn starch-based biodegradable straws. Ind. Crop. Prod. 189. https://doi.org/10.1016/j.indcrop.2022.115881.
Wu, Y., Geng, F., Chang, P.R., Yu, J., Ma, X., 2009. Effect of agar on the microstructure and performance of potato starch film. Carbohydr. Polym. 76, 299–304. https://doi.org/10.1016/j.carbpol.2008.10.031.
Yu, I.K.M., Chen, H., Abeln, F., Auta, H., Fan, J., Budarin, V.L., Clark, J.H., Parsons, S., Chuck, C.J., Zhang, S., Luo, G., Tsang, D.C.W., 2021. Chemicals from lignocellulosic biomass: a critical comparison between biochemical, microwave and thermochemical conversion methods. Crit. Rev. Environ. Sci. Technol. 51, 1479–1532. https://doi.org/10.1080/10643389.2020.1753632.
Zhang, R., Ma, S., Li, L., Zhang, M., Tian, S., Wang, D., Liu, K., Liu, H., Zhu, W., Wang, X., 2021. Comprehensive utilization of corn starch processing by-products: a review. Grain Oil Sci. Technol. https://doi.org/10.1016/j.gaost.2021.08.003.
Zhang, Y., Thompson, M., Liu, Q., 2011. The effect of pea fiber and potato pulp on thermal property, surface tension, and hydrophilicity of extruded starch thermoplastics. Carbohydr. Polym. 86, 700–707. https://doi.org/10.1016/j.carbpol.2011.05.009.
Zhang, Y., Zhao, X., Bao, X., Xiao, J., Liu, H., 2021. Effects of pectin and heat-moisture treatment on structural characteristics and physicochemical properties of corn starch. Food Hydrocoll. 117. https://doi.org/10.1016/j.foodhyd.2021.106664.
Zuo, Y., Gu, J., Yang, L., Qiao, Z., Tan, H., Zhang, Y., 2013. Synthesis and characterization of maleic anhydride esterified corn starch by the dry method. Int. J. Biol. Macromol. 62, 241–247. https://doi.org/10.1016/j.ijbiomac.2013.08.032.
Zuo, Y., Gu, J., Tan, H., Qiao, Z., Xie, Y., Zhang, Y., 2014. The characterization of granule structural changes in acid-thinning starches by new methods and its effect on other properties. J. Adhes. Sci. Technol. 28, 479–489. https://doi.org/10.1080/01694243.2013.843283.
Zuo, Y., Liu, W., Xiao, J., Zhao, X., Zhu, Y., Wu, Y., 2017. Preparation and characterization of dialdehyde starch by one-step acid hydrolysis and oxidation. Int. J. Biol. Macromol. 103, 1257–1264. https://doi.org/10.1016/j.ijbiomac.2017.05.188.